The Thesis Committee for Nazmus Sakib
Certifies that this is the approved version of the following thesis:

Response of Asphalt Matrix under Multi-axial Stress State

APPROVED BY
SUPERVISING COMMITTEE:

Supervisor:

Amit Bhasin

Andre d.F. Smit

Response of Asphalt Matrix under Multi-axial Stress State

by

Nazmus Sakib, B. S.

Thesis

Presented to the Faculty of the Graduate School of

The University of Texas at Austin

in Partial Fulfillment

of the Requirements

for the Degree of

Master of Science in Engineering

The University of Texas at Austin

May 2014

Dedication

Dedicated to my family.

Acknowledgements

At the beginning, I want to thank my mentor, Dr. Amit Bhasin for his continuous support and inspiration. With his constant guidance, acclimatizing with Austin has been a pleasant experience, personally and academically. It has been a great privilege to work under his supervision, as he was available to me for any sort of situations that may arise during the research and personal life.

I would also like to thank Dr. Andre Smit to his thoughtful guidance during the preparation for this thesis. His suggestions guided me to look into my own work through the perspective of the readers. His enthusiasm inspired me to pursue further detailing of the thesis.

I want to thank my friends who, despite being far, had helped me to keep my foot on the solid ground. The reminiscence of the fun we had together has always been my source of solace.

I want to express my deep gratitude towards the government and the people of Bangladesh for supporting the financial burden of my education, from the first grade to the tertiary level. I stand humbly before the sacrifice the country had to make for my betterment.

Finally, I would also like to express my gratitude to my family. I am specially indebt to my newlywed wife. She had to endure my absence while writing this thesis. I want to thank my parents for their support throughout my life and never giving up on me.

Abstract

Response of Asphalt Matrix under Multi-axial Stress State

Nazmus Sakib, M.S.E

The University of Texas at Austin, 2014

Supervisor: Amit Bhasin

The pavement system is subjected to complex stress states under vehicular loading. A combination of axial and shear stress has been identified as a potential cause of top down cracking (or more precisely near surface cracking) in asphalt surface. Therefore, in terms of modeling the material response a pertinent question is whether the typical one-dimensional viscoelastic properties of the material are affected by a multi-axial stress state. Such changes are referred to as interaction non-linearity. The objective of this study was to evaluate whether or not asphalt composites are susceptible to such interaction effects. The study was conducted using fine aggregate matrix (FAM), which comprises graded sand and asphalt binder.

To provide multi-modal loading, the rectangular prismatic FAM specimens were used with the Arcan apparatus. This apparatus ensures low bending stress and offers adjustments in the setup to provide different proportions of axial and shear stress. Finite element modeling was done to evaluate the stress state for different orientations of the sample in the Arcan apparatus. For measurement of strain, the study used digital image correlation (DIC), which is an optical, non-contact measurement technology. The strain thus measured was used to compute shear compliance. Fitting parameters of the shear compliances were estimated for power-law and Prony series for different loading

orientations. When compared, the measured shear compliances do not show perceivable variation with respect to different proportion of axial stress applied in conjunction. However, further testing with different temperatures and other magnitudes of shear stress is necessary. This study is the first step to allow modeling of stress and crack propagation behavior near the pavement surface where complex stress state is present.

Table of Contents

List of Tables

List of Figures

Chapter 1: Introduction

SCOPE OF WORK

Asphalt mixture is a heterogeneous composite comprising different sizes of aggregates and asphalt binder along voids filled with air. The coarser fraction of the aggregate makes up bulk of the volume and imparts strength to the mix while the binder acts as a glue to adhere the granular parts of the asphalt mix. The fine portion of aggregates and the binder with air can be defined as the mortar or matrix of the composite in which the coarse particles are embedded. Under vehicular loading, this composite helps transfer the load to the lower layers of the pavement.

Being heterogeneous in nature, the study of asphalt mixtures poses several challenges. The main components of the mix, aggregates and binder, are two very different types of material, the former being elastic and the latter being viscoelastic. As a viscoelastic material, asphalt binder is sensitive to temperature and rate of loading. For these reasons, the study of the asphalt pavement requires diligent attention to the properties of the constituent materials of the asphalt composite as well as the properties of the asphalt itself with respect to factors such as loading rate, temperature, and state of stress within the pavement. As a heterogeneous mixture of particulate nature, asphalt can show anisotropy or directional variation of properties. Confining stresses and deviator stresses within the pavement can contribute to the variance of material properties exhibited by asphalt composite.

Traditionally, flexural tensile stress was thought to be responsible for load-induced pavement cracking. The strength of the material, combined with the tensile stress at the bottom of the asphalt layer in a pavement structure is typically used to evaluate the capacity and performance of the pavement system. In other words, flexure causes tensile stress at the bottom of pavement layer and tensile fatigue, caused by the repetition of tensile stress, is responsible for classic bottom-up cracking.

However, researchers have also reported that cracks do not necessarily start opening up from the bottom of the asphalt layer; cracks can initiate and propagate starting from the top of the pavement layer as well. This phenomenon was termed as Top Down Cracking (TDC). In fact, in the more recent studies, TDC has been shown to originate not from the top surface of the pavement, but from slightly beneath the top surface. Hence, it is referred as Near Surface Cracking as well.

Researchers have identified several causes for TDC while attributing overall elevated state of stress at the point of crack origin as the most important factor. The term 'state of stress' indicates localized combination of stresses (axial and shear) near the pavement surface. Combinations of the stresses can cause tensile stress of such magnitude which can initiate and propagate cracks, as found in some studies. These types of cracks are referred to as Type I cracks, being tensile in nature. Importantly, TDC is also identified by some researchers as a Type III crack indicating a mixed mode cracking type (combination of tensile and shear) (Ozer et al., 2011).

As mentioned before, the coarse portion of the asphalt mix (coarse aggregates) imparts strength and volume to the mix while asphalt binder, in combination with fine aggregates,

provides the mortar to bind the aggregates as a matrix of the composite. The fine aggregate matrix (FAM or sand-aggregate mix or asphalt mortar) is vulnerable to damages related to its viscoelastic nature. As the coarse aggregates carry the major portion of the load by mechanical interlocking, they are subjected to displacement under loading. FAM stays within the inter-aggregate space bonding the coarse aggregate particles.

Numerous studies were conducted to evaluate the direct tensile strength of asphalt mix and FAM. These studies are applicable for predicting Type I cracks' initiation and propagation. However, material properties of asphalt mix and FAM under mixed mode loading are not readily available due to lack of studies.

PROBLEM STATEMENT

The state of the art recognizes the presence of mixed mode stress in pavement. In addition, creation of near surface cracks due to such stress scenarios is also acknowledged. However, in current practice, asphalt composite under mixed mode state of stress is assumed to exhibit the same stress-strain relationship (creep compliance) as it would do in the case of pure tensile or shear loading.

Interestingly, a few studies (Motamed et al., 2011, 2012) show that the behavior of the binder is altered to some extent in the presence of mixed mode loading. For this reason, characterizing the behavior of asphalt mix under mixed mode loading is essential.

As FAM has a higher proportion of viscoelastic binder than for a full asphalt composite, any change of the material property due to the mixed mode stress would be more notable.

For asphalt with coarse aggregates, the granular structure of the coarse aggregates can vary from specimen to specimen and exhibit variation of strength. Hence, the effect of stress state on material properties may be masked under the specimen-wise variation of strength. FAM provides more material uniformity than the asphalt and specimen-wise strength variation should be comparatively small. Therefore, evaluating the strain response of FAM in the form of creep compliance would help to identify the presence of possible alteration under mixed mode stress.

HYPOTHESIS

The purpose of the test would be to identify the variation in shear creep compliance of FAM, if any, for different combinations of shear and axial stresses. For a constant value of shear stress (σ_{xy}) in the FAM specimen, the magnitude of axial stresses (σ_{xx} and σ_{yy}) would be altered and corresponding shear strains (τ_{xy}) would be measured. Thus, any change of creep compliance for shear for different axial stresses but same shear stress would indicate that FAM is sensitive to mixed mode of stress.

OBJECTIVE OF THE STUDY

The objective of the study is to identify variation of shear strain with respect to different magnitudes of axial stresses. To achieve this overall objective, the following specific targets have to be accomplished:

- Choosing a specimen geometry such that a sufficient gauge length with a uniform stress profile exists

- Developing a test setup/apparatus which enables mixed mode loading on the specimen
- Creating a finite element model of the test to obtain the stress tensor in a given location of the sample
- Adopting a practical and accurate strain measurement technique considering data requirements and specimen geometry
- Conducting a single cycle loading-unloading/creep recovery test and comparing the measured strain profiles and resultant creep compliances for different loading scenarios

THESIS OUTLINE

The study is divided into five sections. After the current section defining the scope of the research, a literature review is conducted. The literature review touches on the causes of TDC, and discusses the significance of the complex stress state in this case. In this section, previous studies focusing on the existence of variable shear compliance for different axial stress is discussed in detail. This section also contains a discussion on FAM and available mixed-mode loading techniques. A comparatively new technology for strain measurement using optical techniques, called Digital Image Correlation (DIC), is also discussed. In Chapter 3, the narrative includes the preparation of the FAM specimen, detailed discussion of the testing apparatus and strain measurement technique. Chapter 4 is focused on developing a finite element model and from the model, marking out the zones of uniform stress in the specimen for two different specimen geometries.

The chapter touches on the relative preference between these two geometries and establishes the loading parameters to be implemented during the actual test. The penultimate chapter contains a brief discussion on the test and details the findings from the test. Finally, concluding remarks are made while identifying the limitations of the current study and potential future research topics.

Chapter 2: Literature Review

In this chapter, the discussion on the complex stress states in the asphalt pavement precedes a discourse on the material behavior. Different theories on Top Down Cracking (TDC) initiation and propagation are presented followed by the relation between TDC and complex stress states. This is followed by a discussion on the methodologies used to investigate the influence of multi-axial stress state on the properties of asphalt mortar and the findings from this investigation. Then, studies involving the choice of test material are overviewed along with the available testing apparatuses, which enables mixed-mode loading on asphalt samples. Finally, strain measurement techniques are discussed and choice of digital image correlation is validated.

CAUSES OF TOP DOWN CRACKING

Traditionally, bottom up or flexure cracking was thought as the primary fatigue distress in the asphalt pavements. Flexure cracking is a well-researched and a relatively easy mechanism to understand. However, researchers found the evidence that not all cracks are related to bottom-up cracking. A different type of cracking, called Top Down or Near Surface Cracking, is identified and correlated with the complex stress state within the pavement structure.

Gerritsen et al., (1987)observed cracks to originate from near the surface and appear 3 to 5 years after construction. Similar observation was also made by Dauzats and Rampal (1987)identifying thermal stress as a potential cause of such cracking. Matsuno and

Nishizawa (1992) observed surface cracking in Japan. They identified that the cracks are in proximity to the wheel path. They also identified that the temperature of the pavement can be a contributing factor as cracking was not observed under overpasses or tunnels, i.e. the areas without sunlight.

Researchers from University of Florida conducted comprehensive tests on eight pavement sections, aged 5 to 10 years(Myers et al., 1998). It was observed that the cracks were 3 to 4 mm wide at the surface. The observation indicated tensile mode of failure (Type I fracture) as found by Matsuno and Nishizawa (1992).Studies conducted by Ann Myers et al. (2001) and Roque et al. (2010)stated poor fracture resistance as a factor responsible for TDC.

Uhlmeyer et al. (2000) conducted field observation of selected cracked pavements in Washington State. The authors concluded that occurrence of TDC more frequent in thicker pavements and they identified 160 mm thickness as the cutoff for such phenomena to occur. However, Matsuno and Nishizawa (1992) and Myers et al.(1998) did not find any such relation between cracking and thickness of pavement.

Other researchers included pavement construction, aggregate grading, truck tire grooving etc. as potential cause of top down cracking. The factors can be subdivided into load – induced factors (tension, shear), material aging, construction related factors (segregation and joints) and thermal stress (Baladi et al., 2003). However, most of the researchers agree that localized stresses are important contributors to TDC initiation and propagation.

EFFECT OF STRESS-STATE IN THE PAVEMENT ON TDC

As researchers understood the significance of localized stress, they focused on identifying the specific type of stress that causes TDC. Laboratory tests as well finite element modelling techniques were employed for this purpose.

Tensile stress under the ribs of radial tires are identified as a cause of TDC (Myers et al., 1998). In other words, TDC was seen as a Type I fracture. It was found that a secondary tensile stress may be generated by dilation of asphalt under shear loading (Wang et al., 2003). In another study, it was found that vertical shear strain near the edges of a tire causes a more severe stress condition and thus it has the potential to initiate top down cracking (Wang and Al-Qadi, 2010). The study identified high temperature as an important factor and found that the cracks can initiate between dual tires near the surface.

Researchers has also pointed out that the current approximation of uniformity of stress under tires is not applicable for TDC analysis. They observed significant stress increases due to the pressure of ribs in tires. Wang (2009)observed that consideration of the rib effect on contact stress will cause much higher stress levels in pavement. Using finite element modelling, it was found that the magnitude of maximum vertical stress when considering rib effects (non-uniformity) is about two times higher than that when only considering uniform vertical loading. This phenomenon is more pronounced in the top half inch of AC layers but becomes uniform with depth.

Wang (2011) used FEM to demonstrate that load distribution under a tire is dependent on load, tire inflation pressure, vehicle maneuvering (breaking, acceleration, cornering), and rolling condition (slip angle, friction). Different tires can produce different stress states in

the pavement. Wang (2009) identified that the location of maximum (principle) tensile and shear stress and their magnitude varied with the type of tire.

In the above mentioned studies of Wang (2009) and Wang (2011), development of mixed mode stress state (tension with shear) was prominent. Figure 2.1 is a graphical representation of spatial variation of the stress state near the surface of the pavement when subjected to wheel load from a ribbed tire. Intuitively, the presence of mixed mode stress states in the pavement elements can be understood from this figure, which shows various combinations of tensile, compressive and shear stresses at different locations in the pavement under the tire.

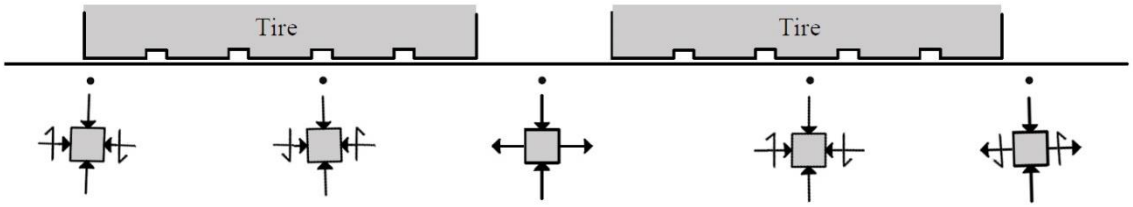

Figure 2.1: Multi Axial Stress State under Tires

More importantly, Ozer et al. (2011) identified mixed mode fracture (Type III) as a critical case. They conducted 3D finite element modeling (FEM) of a typical pavement structure with thick bituminous layer and inserted different shapes of crack within this model. They also mentioned that the tensile mode of failure can be found at 30-60 degree planes (crack angels) and at about 60 mm depth from the surface. The researchers also found that the most critical orientation of cracks appears to be in the 45 to 60 degree

range with the vertical plane. The researchers concluded that tensile mode of fracture cannot properly predict the TDC scenarios. For this reason, they identified mixed/complex mode (shear with compression) as the prominent contributor to near surface damage of the pavement.

MATERIAL BEHAVIOR UNDER COMPLEX STRESS-STATE

Under a complex multi-axial stress state (tension/compression-shear combination), the material properties of an asphalt mix can be different from the properties measured under uniaxial tension/compression or shear. Some materials are known to possess interaction non-linearity, which refers to the variation of material properties with respect to state of stress within the material.

An example of interaction nonlinearity can be seen in Polymethyl Methacrylate, which exhibits a different shear compliance for different states of stress (Lu and Knauss, 1998). Polymethyl Methacrylate is a thermoplastic, commonly known as acrylic glass or Plexiglass or Perspex. In the mentioned study, pure shear creep was measured at different temperatures. These tests were repeated with the same shear load along with an additional compressive or tensile load. The study indicated “a marked influence” of the axial loads on shear creep. The study found that the positive invariant (tension with shear) produces higher creep compliance than negative (compression with shear). Figure 2.2 shows this difference.

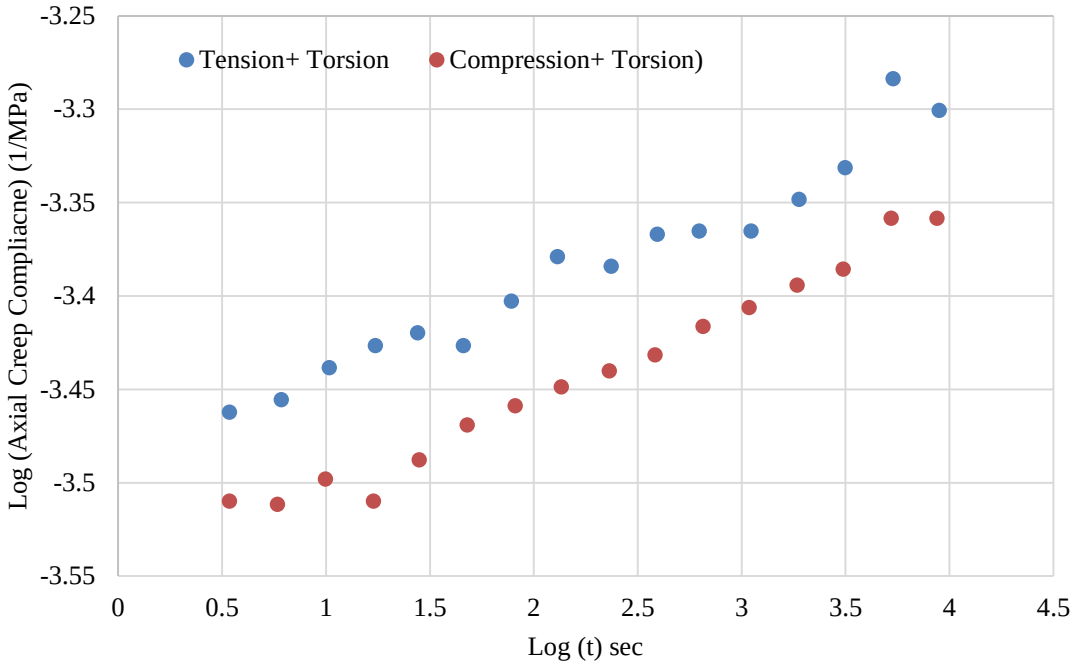

Figure 2.2: Creep Compliance for Torsion with Tension and Shear (adopted from Lu and Knauss, 1988)

When subjected to similar complex stress states, asphalt binder exhibited similar behavior (Motamed et al., 2011, 2012) . The test data indicated that a compressive normal force was generated during the application of torsional shear. The dynamic shear modulus was found to reduce corresponding with an increase in the normal stress. In this study, researchers conducted a stress sweep test on PG 82-22 binder at 40ºC. The binder was placed between a fixed bottom plate and a rotating top cone plate and was subjected to sinusoidal oscillation at0.1 Hz. A slower loading rate was chosen to exaggerate the time dependent properties of the binder. Stress amplitudes were varied from 100 Pa to 48.1 kPa. Other studies have shown that the binder behaves linearly at this stress level

(Delgadillo, 2008; Huang, 2008). Motamed et al. (2011, 2012) observed the generation of a normal force when the specimen was confined in the vertical direction. It was also noted that the complex modulus varied with stress levels as shown in Figure 2.3.

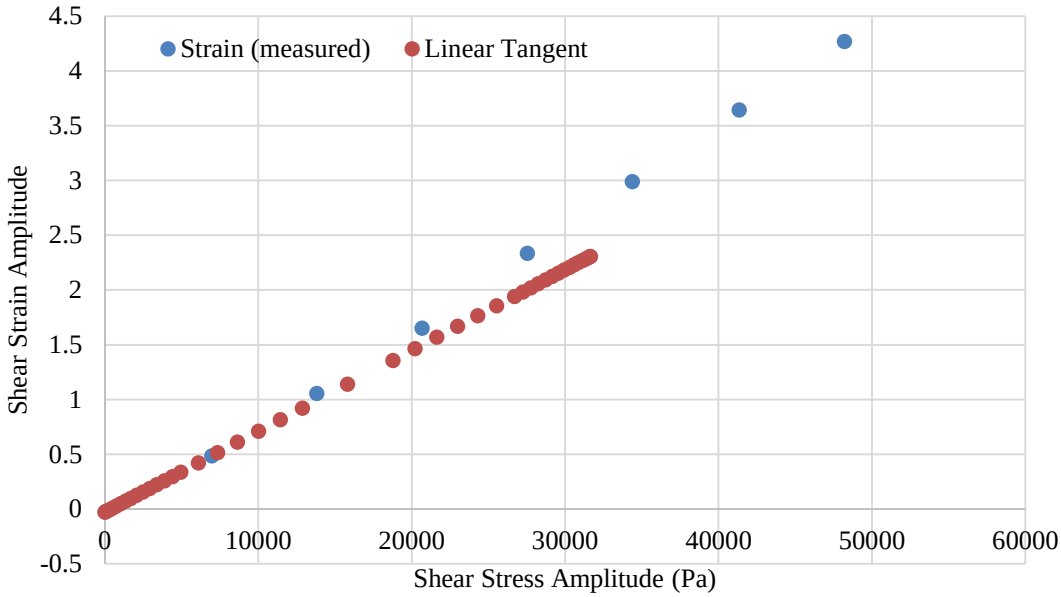

Figure 2.3: Variation of Shear Modulus and shear strain w.r.t Shear Stress Amplitude

Figure 2.3 shows that there is slight deviation from linearity as the shear stress increases. The researchers considered two possible causes: the Poynting effect due to geometric nonlinearity (Poynting, 1909) and interaction non-linearity. The researchers concluded that the Poynting effect could only partially explain the observed normal force, but that the dilation of the binder due to the shear stress also contributed to the normal force. The presence of the normal force/stress combined with the applied shear stress resulted in a corresponding change in the shear modulus attributed to Interaction non-linearity.

CHOICE OF FINE AGGREGATE MATRIX

As the asphalt binder is used with aggregates to create HMA, it is practical to identify the presence of non-linearity for HMA. However, the use of HMA specimen (full mix) present some challenges for this specific purpose. One of the primary concern is the degree of heterogeneity in HMA. While the heterogeneity is also present in asphalt binder at solution or suspension level, full mix asphalt is heterogeneous at a length scale that is directly relevant for material and pavement structural design. The presence of coarse angular aggregates would create local stresses of unpredictable nature. This highly localized stresses would invalidate the test as we seek to understand strain caused by known combination of stresses. In addition, testing of HMA mix requires a large sample and testing apparatus that was not efficient for use in this preliminary study. Importantly, fatigue or stress related damage in pavement usually initiates in asphalt matrix and typically not in coarse aggregates (of good mechanical properties). Hence, excluding the coarser portion of HMA is a logical and meaningful compromise as a first step to develop a better understanding of material behavior. The resulting composite is effectively the asphalt matrix or fine aggregate matrix (FAM) also referred as sand-asphalt mortar. FAM consists of binder and fine aggregates.

The results obtained by testing full scale specimens of asphalt mix and FAM specimens indicates that the FAM microstructure closely resembles the microstructure of FAM within a full asphalt mix (Izadi et al., 2011). For this reason, we can expect FAM specimens that are designed and produced in the laboratory to exhibit behavior comparable to the asphalt matrix holding coarse aggregates together as in the case of a

full-mix. The mentioned study also states that FAM is less sensitive to percentage of fines than binder content.

FAM offers some advantages over full-scale asphalt mix testing. Since cracking or damage is concentrated in the sand-asphalt mortar, evaluating FAM in isolation can provide a closer look into the failure mechanism. FAM excludes larger aggregates and thereby reduces the heterogeneity of the mix. In addition to that, FAM enables us to reduce the amount of material required and consequently reduces the requirement of high-capacity equipment due to the small-scale for testing. These qualities render FAM to be a more economical material. For these reasons, FAM received preference over the full-mix asphalt for the current study.

While previous studies have demonstrated that asphalt binder exhibits interaction non-linearity (Motamed et al., 2011, 2012), the same cannot be conclusively said about asphalt mortar. The behavior of asphalt mortar can be different from that of the asphalt binder due to the heterogeneity of the mortar. In addition, the stiffness of the mortar is usually much higher than that of the binder. Since cracks usually propagate through the asphalt mortar within an asphalt mixture, it is critical to understand the response of asphalt mortar subjected to multi-axial stresses as the first step to better understand the behavior and performance of full asphalt mixtures. To the knowledge of the author, no previous research has addressed the interaction non-linearity in asphalt mortar.

TESTING OF ASPHALT SPECIMENS IN MIXED MODE STRESS-STATES

Testing of asphalt specimens under complex loading condition requires special test set-ups. In past, several researchers developed and conducted tests on asphalt samples where shear was a prime consideration. There are several devices that are able to apply direct shear to test specimens. Among these test procedures, some of the more notable ones are Layer Parallel Direct Shear Test, Florida DOT device, bond torque test and pull-off test. However, none of these tests can apply a geometrically controlled mixed mode loading on the test specimen.

To fulfill this need, different agencies developed various test equipment, which were capable of imparting axial load along with shear. One of these devices is Ancona Shear Testing Research and Analysis (ASTRA), developed by Polytechnic University of Marche. The device is effectively a direct shear test device similar to the device used for soil shear testing. A specimen is placed into two box shaped grips facing each other which are able to move horizontally in opposite directions. One of the grips can be loaded with weight to produce a normal compressive force (Canestrari et al., 2005). This system allows the sample to fail in shear along a predetermined plane in presence of a compressive load.

Romanoschi and Metcalf (2001) conducted direct shear tests at four levels of normal loading using a specialized setup. Using a single loading frame and by sample alignment, the authors were able to conduct shear fatigue tests where the shear stress was half the normal stress. Figure 2.4 illustrates the principle of this test. Though this test setup is capable of applying a combination of shear and normal force, the ratio of these two

stresses has to be kept constant. This apparatus also loads the sample along a predetermined plane.

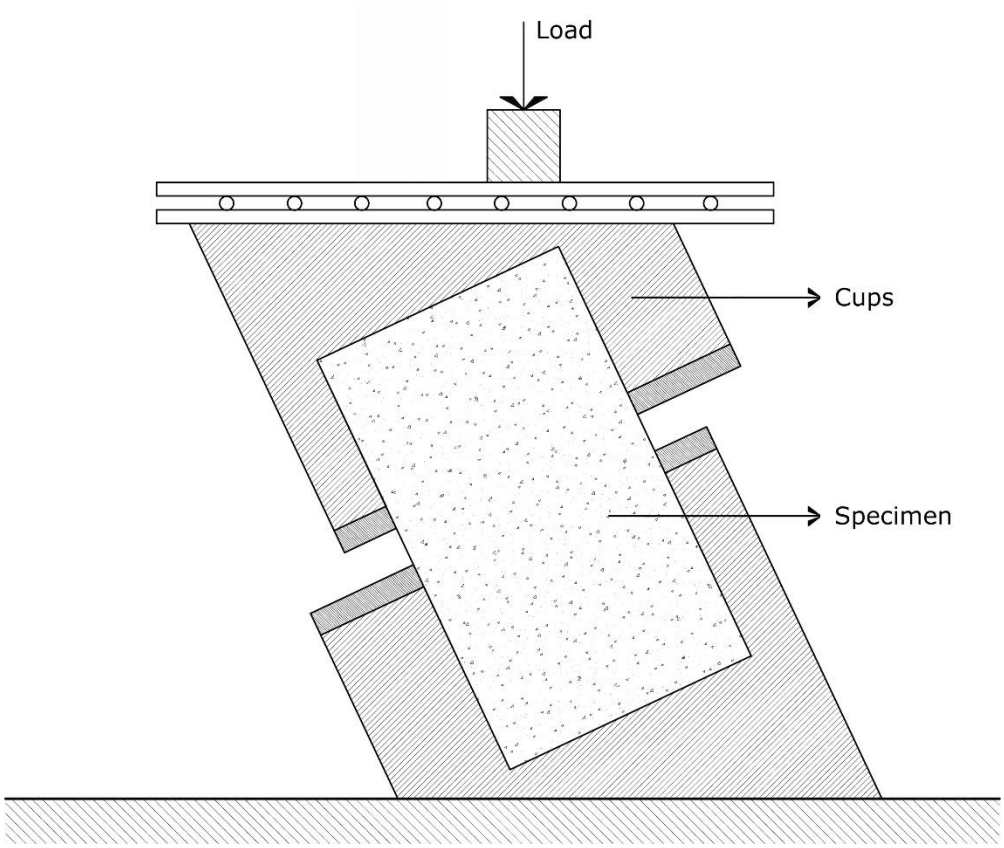

Figure 2.4: Direct Shear with Normal Load Test Setup by Romanoschi and Metcalf (2001)

The test device that could apply a multi axial stress state that also gained the most attention was the Superpave Shear Tester (SST). This device was used to measure the complex shear modulus and the permanent deformation characteristics of asphalt mix in shear. Figure 2.5 shows the schematic of the SST. The bottom attachment is able to

produce shear loading while the top attachment to the sample produces normal loading. This apparatus is able to produce different combinations of mixed mode loading without a predetermined failure/loading plane. Also due to the size of the sample, there would be bending effects caused by shear which would negate the pure shear assumption. Owing to high cost and complexity of operation and maintenance the SST was not widely adopted for routine use or even as a research tool.

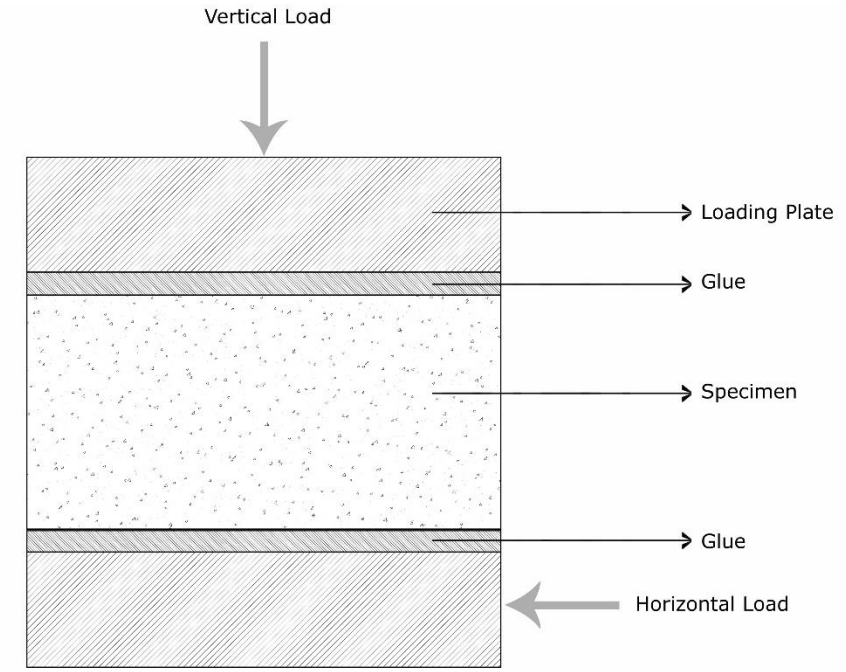

Figure 2.5: Basic schematic of Superpave Shear tester

The aforementioned setups are capable of applying mixed mode loading to some extent. However, for the purpose of this study, these setups were not advantageous because they cannot provide mixed mode loading with varying magnitudes without causing bending of sample. In addition, all setups except the SST apply load on a specified plane, rather than

a gauge region. Thus, deformation is forcibly limited to a predefined plane of small thickness with high spatial variation of stresses and hence unsuitable for this study. On the other hand, SST would result in a bending effect.

To counter the disadvantages with the available options, two other setups were considered; namely, the Iosipescu and Arcan configurations. Both of these are used for smaller scale samples and more common in the polymer and composite industry. The advantage of these two setups is that they result in a more uniform shear stress on the specimen. Maintaining the uniformity of stress over the gauge length is important to establish the relationship between stress and strain, which is the primary objective of these kinds of tests. Variation of stress within the gauge region would result in corresponding variations in strain and hence the measured deformation would not be proportionate to actual strain. As a result, obtaining accurate strain and correlating stress-strain would be difficult. Uniformity of stress over a larger section of the test specimen would allow the use of a larger gauge length and subsequently reduce measurement errors related to strain gauges and local irregularities.

The Iosipescu configuration (Iosipescu, 1967) is a setup which involves a double V-notch specimen subjected to four-point bending. The Iosipescu configuration has been widely used to study composite behavior. However, for the current study, the Arcan specimen (Arcan et al., 1978) was used, which has some similarity to the Iosipescu specimen. The Arcan specimen is preferable to the Isoipescu specimen because of its low bending effect and the possibility of using multiple orientations of the setup (Hung and Liechti, 1999). This geometry also enables the application of multi-axial loading when used in

combination with UTM, a widely available device. The Arcan setup does not include any bearings and hence there is less possibility of friction related error. These benefits allow the user to achieve a mixed-state loading and a homogeneous stress region for analysis. A commonly used schematic of the Arcan setup is shown in Figure 2.6.

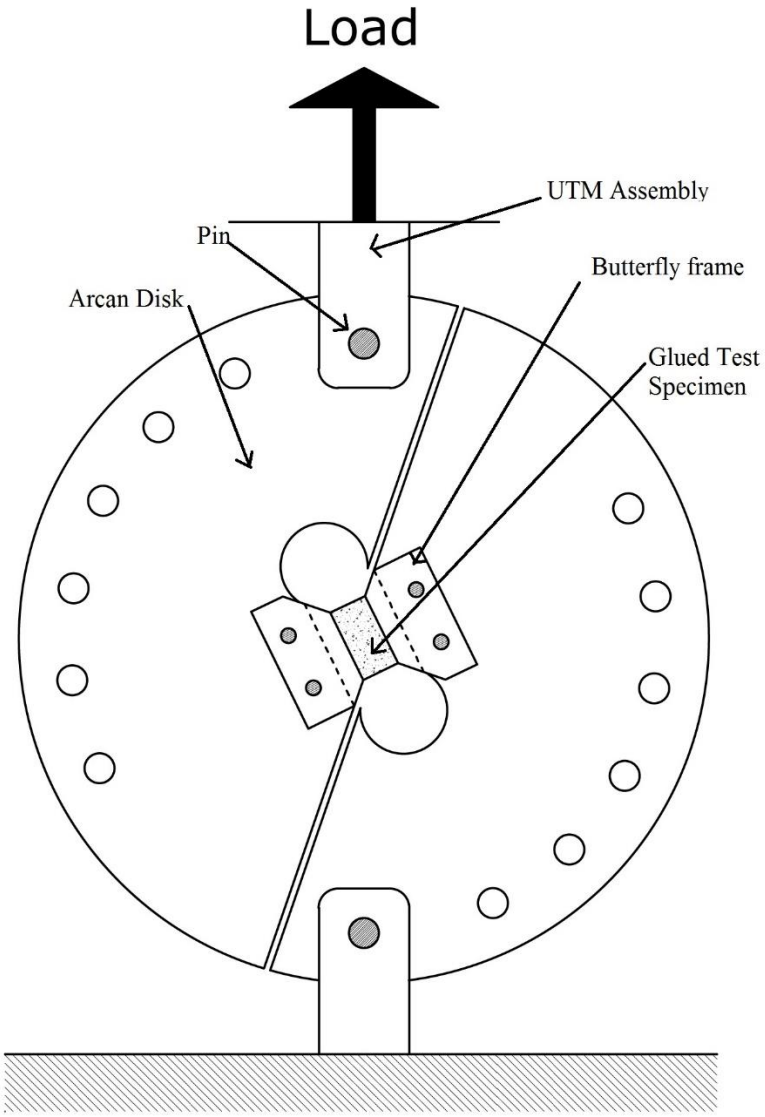

Figure 2.6: Schematic of the Arcan Test Setup

MEASUREMENT OF STRAIN

As stated before, this study involves measurement of strain under complex stress states to evaluate change in material properties, if any, under such stress states. Hence the ability to measure strains accurately was critical to the success of this study.

Commonly used strain measurement techniques are extensiometers and strain gauges. Due to the small size of the FAM specimen (smallest dimension is 10 mm), these techniques were not suitable. Additionally, heterogeneity of the specimen, the requirement of at least three strain gauges (strain rosette) for measuring shear and axial strain components, and possible misalignment and localized damage during placement of the gauges makes the use of such techniques less preferable.

For these reasons, full field no-contact strain measurement techniques present a better alternative. Some of these techniques are interferometry, Moiré interference, and brittle coating. However, a relatively new technology, Digital Image Correlation (DIC), was employed in this study. DIC was first proposed around 1980s (Schreier et al., 2009; Sutton et al., 2000) but has become increasingly popular in recent years due to the availability of high speed desktop computers. Despite being a full field technique, DIC is capable of point measurement of strain similar to strain gauges. For this study, a DIC-based commercially available optical measurement software, VIC-3D™, was used.

According to the literature, the 3D DIC technique provides dependable strain and displacement measurements (Sutton et al. 2000). The system used for this study was capable of measuring from 50 micro-strains to 2000% strain for specimen sized less than 1 mm to more than 10 mm (Correlated Solutions, 2013).

Utilization of DIC along with the Arcan setup provides a favorable setup for strain measurement. If the uniformity of stress over a region on the specimen can be confidently established and identified, strain measurement by DIC would be more consistent. Having a uniform stress region would produce results that are more dependable as well as identification of possible discontinuity in the specimen and localized irregularity.

Chapter 3: Experimental Setup

This section describes the experimental procedure that was used to measure the response of an asphalt matrix under complex stress states. In this section, discussion on the preparation of asphalt matrix is followed by the description of the loading apparatus, the Arcan apparatus. Preparation of the specimen is also discussed. In this research, a relatively new technology of strain measurement based on digital image correlation is utilized. A discussion on this technology is included in this chapter.

PREPARATION OF ASPHALT MIX

All tests in this study were conducted on asphalt mortar or fine aggregate matrix (FAM). FAM comprises of asphalt binder and fine aggregates. For the binder, we selected PG 67-22 grade bitumen. The fine aggregate originated from a limestone quarry in Bryan, Texas. These aggregates pass through ASTM Sieve no. 16 (smaller than 1.18 mm). Table 3.1 shows the gradation of the fine aggregates.

Sieve Size (mm)	1.18	0.6	0.3	0.15	0.075	0	Ret.
Sieve Number (#)	#16	#30	#50	#100	#200	-200/ Pan	%
% of Aggregates Retained	0.00	21.0	12.0	9.0	10.5	10.5	63.0

Table 3.1: FAM mix proportions

For this gradation, 63% of the total aggregates pass through ASTM Sieve no. 16 and the remaining portion retains on the sieve, hence excluded from the FAM mix. This

gradation represents the fine aggregate portion of a dense graded asphalt mix. In other words, proportions of the different aggregate sizes and binder in the FAM correspond to the dense graded asphalt mix without coarse particles (larger than 1.18 mm). FAM has the same binder content (weight ratio of the binder to the available fine aggregates) as the full asphalt mix, excluding the binder absorbed by coarse aggregates in the case of the full asphalt mix (Izadi et al., 2011).

After mixing the binder and aggregates at 200ºC, a Super-pave Gyratory Compactor was used to compact the mix to 150 mm diameter and 75 mm high cylindrical specimens. A finished cylinder was cut into 10 mm slices along the normal of the cylindrical axis. Figure 3.1 shows 10 mm thick slices. The 10 mm slices from the finished cylinder were then cut to the required specimen size using a rotating blade. Figure 3.2 shows the cutting process and Figure 3.3 shows the finished specimens.

Figure 3.1: 10 mm thick slices from FAM cylinder

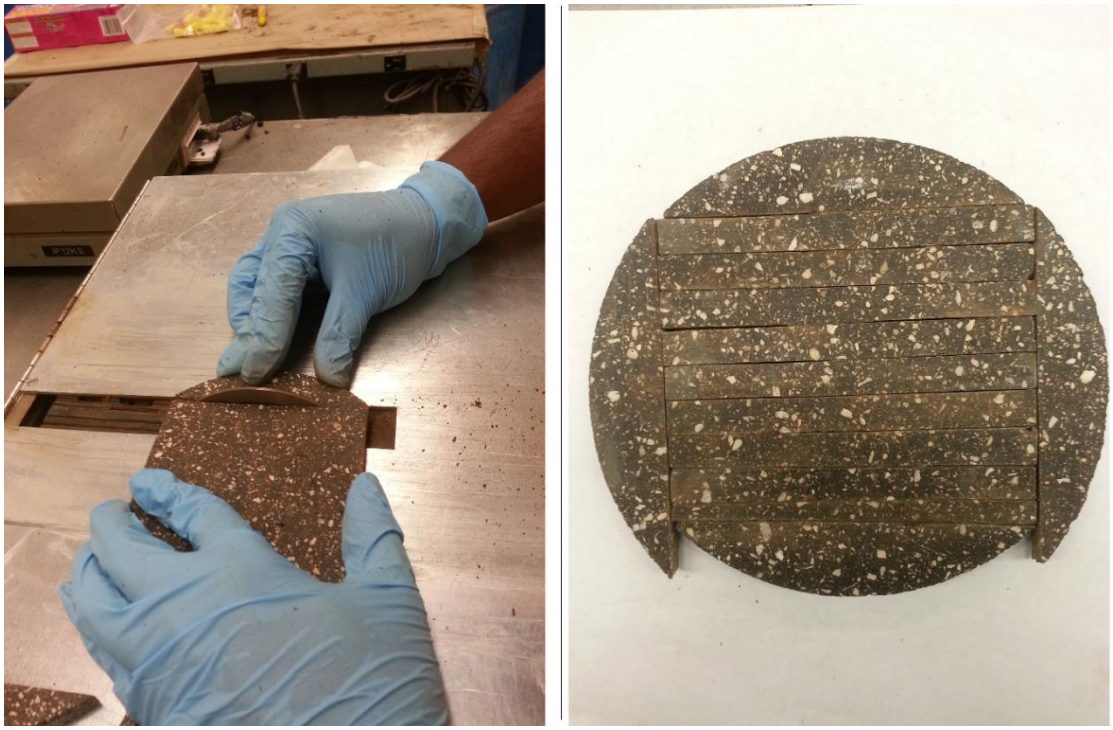

Figure 3.2: Specimen cutting process

Figure 3.3: Finished FAM specimens

ARCAN APPARATUS

This study involves obtaining material properties from observation of the stress-strain behavior under a multi-axial stress state. Ensuring the uniformity of stress within a reasonable gauge length would result in a more reliable measurement of the stress-strain behavior and consequently a more reliable estimate of the constitutive relationship for the material.

An Arcan specimen is usually butterfly shaped with notches at the ends to ensure uniformity of stress. Notches can be V-shaped, rounded V, or semi-circular. In this study, we used rectangular-shaped specimen. The specimen was 10 mm wide and 10 mm deep with an end-to-end length of 23 mm.

The decision to exclude the notch was made in order to simplify specimen preparation and reduce damage to the specimen. Trial specimens of FAM with notch showed problems with replicating the geometry and development of cracks in the corners during creation of the notch. Initially, 5 mm diameter semicircular notch was put on the specimen ends using a punch specially made for this purpose. However, generated force and vibration during punching process caused the edges of the notch to crack and disintegrate. After that, a core drill of 5 mm external diameter with diamond bit was used to make the notch. In this case, the edges did not disintegrate as much as the punching process. However, the heat produced during the drilling made the notch edge quite soft and deformed the shape of the specimen. Observing the difficulty of notch creation, a study was conducted to see the potential of excluding the notch but maintaining a uniform stress region. In the following chapter of this thesis, a comparative study shows

that the uniformity in stress distribution over the gauge length was not significantly affected by removing the notch.

A high strength epoxy was used to glue the Arcan specimen to the loading apparatus. Figure 3.4 demonstrates the glued specimen mounted on the butterfly-shaped frame in preparation for the Arcan Setup.

Figure 3.4: Specimen glued on the butterfly setup

The epoxy presented a particular problem, as it does not adhere to asphalt binder very well. As FAM has higher binder content, the adhesion was not as good as the full asphalt mix where epoxy can bond with coarse aggregate surfaces. However, this particular thixotropic epoxy (DEVCON® 5 Minute® Epoxy Gel) was fast setting (10-15 minute) and rapid hardening (1.5 hour for functional cure). During testing, there are several cases of stripping of epoxy from the FAM specimen. This has been a critical factor for limiting the magnitude of load application. This problem was identified at later stages of study. However, a possible solution is to use a silicon-based epoxy which takes 2 days to cure.

This alternative was not chosen due to limited time and required number of the required butterfly-frames. This is because the specimen would occupy the butterfly frame for longer duration and would require larger number of butterfly frames to utilize time efficiently.

The loading apparatus consists of semi-circular aluminum plates with holes around the edges, which facilitate attaching to the Universal Testing Machine (UTM). The Arcan specimen connects the two parts of the Arcan apparatus. The final setup looks like a circular shaped disk consisting of the two parts of the apparatus with an Arcan specimen placed in between. The disk can be rotated with respect to the UTM grips to achieve different combinations of axial and shear loading. Figure 3.5 shows a test-ready Arcan setup with a notched specimen aligned at 45º with the loading axis of UTM.

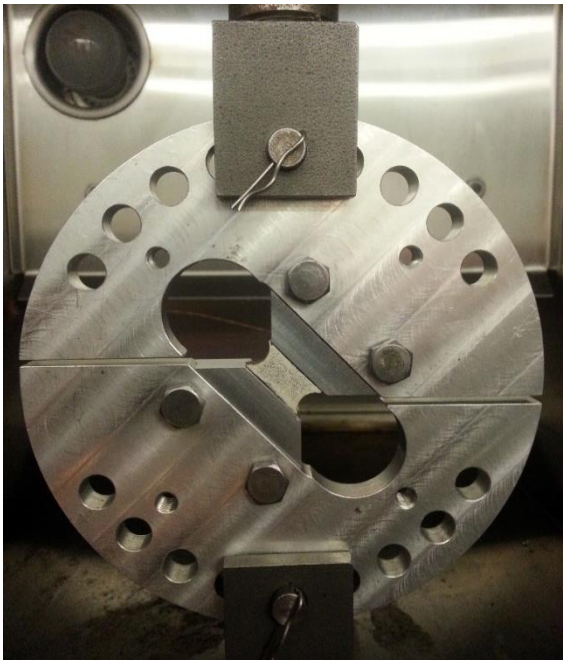

Figure 3.5: The Arcan setup with a notched specimen

STRAIN MEASUREMENT

As discussed in literature review, measurement of strain through the digital image correlation method is critical to this experiment. A well-known DIC software package by Correlated Solutions, Inc., VIC-3D™ is employed for strain measurement.

The complete DIC system consists of two tripod-mounted cameras and VIC-3D™ software. It can provide full field, 3D measurements. The principle of 3D DIC relies on the principle of binocular stereovision (Luo et al., 1993). The system comprises two digital cameras for stereoscopic image acquisition and a post processor for image analysis. The sample to be imaged is generally textured using a speckle pattern with high contrast. The digital cameras capture images of the textured surface at predetermined time intervals. A region of interest (ROI) is defined in the post-processing software to conduct analysis and obtain strain fields. By comparing the location of a specific point/set in consecutive photos during loading, the software establishes the displacement of that point/set. After calculating the relative movements of several points in the ROI, the software computes the strain at those points. A 2D DIC can also be used for planer surfaces with a single camera. However, a 3D DIC enables use of rough surfaces and irregular shapes.

DIC technology is perfectly suited for the purpose of this study. Due to the small specimen size, the measurement of strain using conventional methods was not feasible. Space constraints make it hard to place traditional strain gages on the specimen. In addition, traditional strain gages can track the strains only along a limited number of directions. Moreover, any localized discrepancy or specimen irregularity would not be

pronounced for traditional strain gages. As FAM is a heterogeneous material, localized discontinuity is natural. DIC helps to fully monitor such an experiment where we do not know spatial heterogeneity a priori (Hild and Roux, 2006).

The post-processing software requires sufficient texture to identify and track the deformation in the ROI. For this reason, we painted the surface of the specimen in black and sprayed white paint to incorporate sufficient texture. Figure 3.6 shows the 3D DIC arrangement. Figure 3.4 also shows the FAM specimen with white and black texture. A screenshot of the VIC-3D™ program showing the mounted specimen being analyzed for strain and displacement is presented in Figure 3.7.

Figure 3.6: A 3-D two-camera DIC setup and loading frame (Instron 8872 UTM)

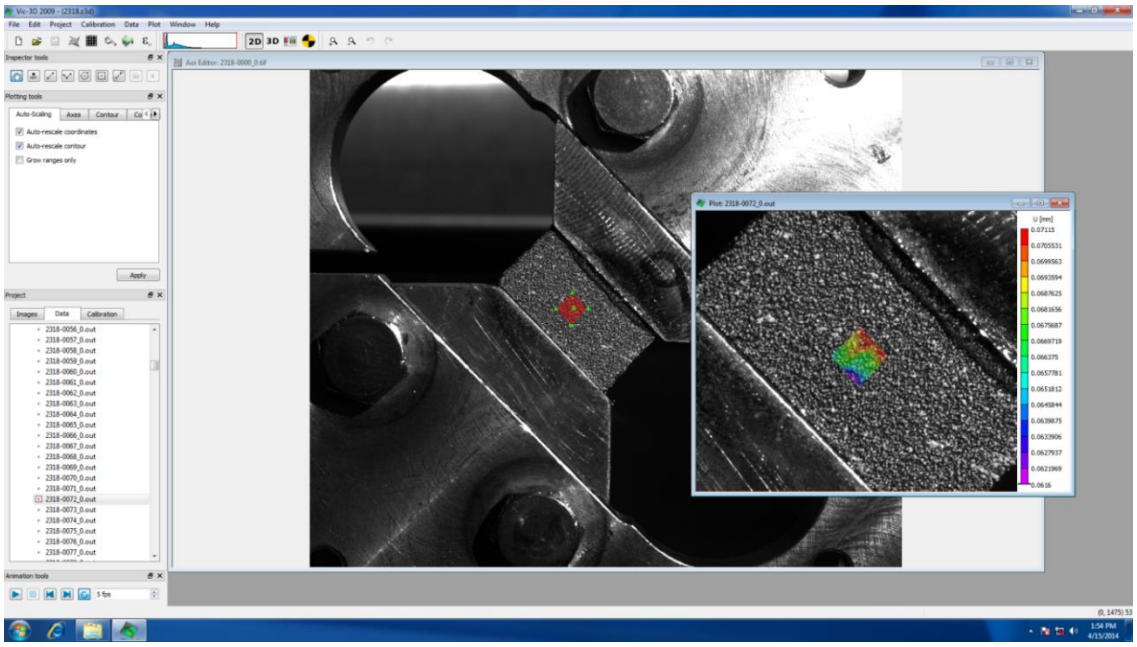

Figure 3.7: A screenshot of strain analysis in DIC

VIC CALIBRATION

Before analyzing any image sequence for deformation in VIC-3D™ system, it requires calibration for a given set of focus, line of sight, and spatial location of the cameras. Calibration is required anytime the system is moved or re-focused. As the specimen is very small, the cameras were placed close to the specimen as seen in Figure 3.6. After that, a calibration target (of known dimensions and texture, provided by the manufacturers of DIC system) is placed in the UTM machine where the Arcan setup would be placed and the focus is adjusted. Figure 3.8 shows a target placed in the apparatus.

Some photos (about 15 to 20) are taken with different orientations of the calibration target with varying rotations and positions within the lenses' depth of field. These images

are used for calibration. The whole calibration process is done as per the suggestion of the developers of VIC-3D™ (Correlated Solutions, 2005). This calibration helps the software to understand the relative location of the individual cameras in space and their line of sight along with focal properties. Figure 3.9 shows the screen shot of the calibration target (focused and analyzed) in the software. Typical information related to the placement of the camera obtained from the calibration is presented in Table 3.2.

Camera Intrinsics		
	Camera 1	Camera 2
Center (X)	1525.853 +/- 1513.963	1525.853 +/- 1513.963
Center (Y)	1000.537 +/- 965.420	1000.537 +/- 965.420
Focal Length (X)	7036.361 +/- 3008.333	7036.361 +/- 3008.333
Focal Length (X)	7014.402 +/- 2990.308	7014.402 +/- 2990.308
Skew:	5.687 +/- 4.840	5.687 +/- 4.840
Kappa 1:	-0.324 +/- 0.000	-0.324 +/- 0.000
Camera Extrinsics		
Angles	X	-0.023 +/- 0.000
	Y	12.951 +/- 0.002
	Z	-0.298 +/- 0.000
Distances	X	-41.552 +/- 0.066
	Y	0.001 +/- 0.009
	Z	0.685 +/- 2.902

Table 3.2: Camera placement and orientation information

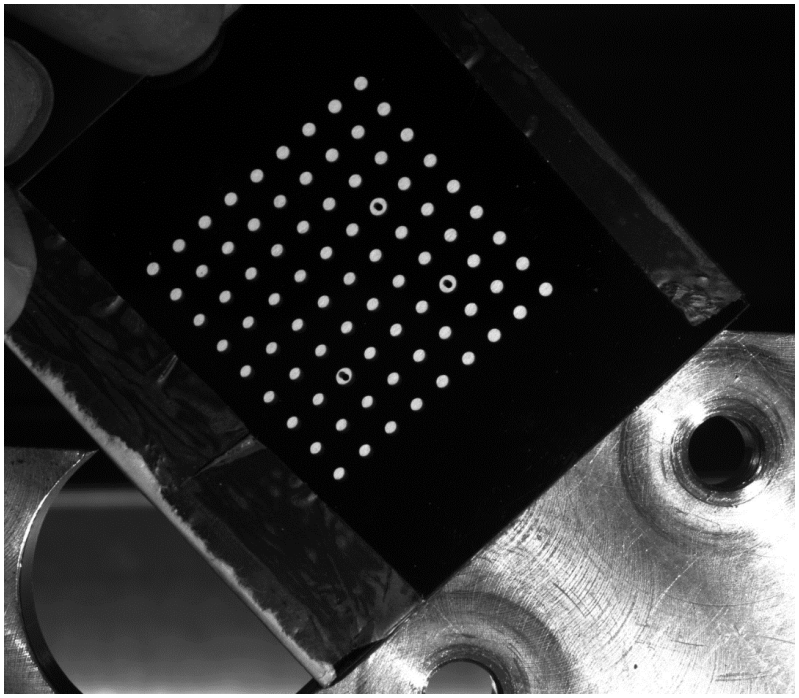

Figure 3.8: Calibration target at the probable location of the test specimen

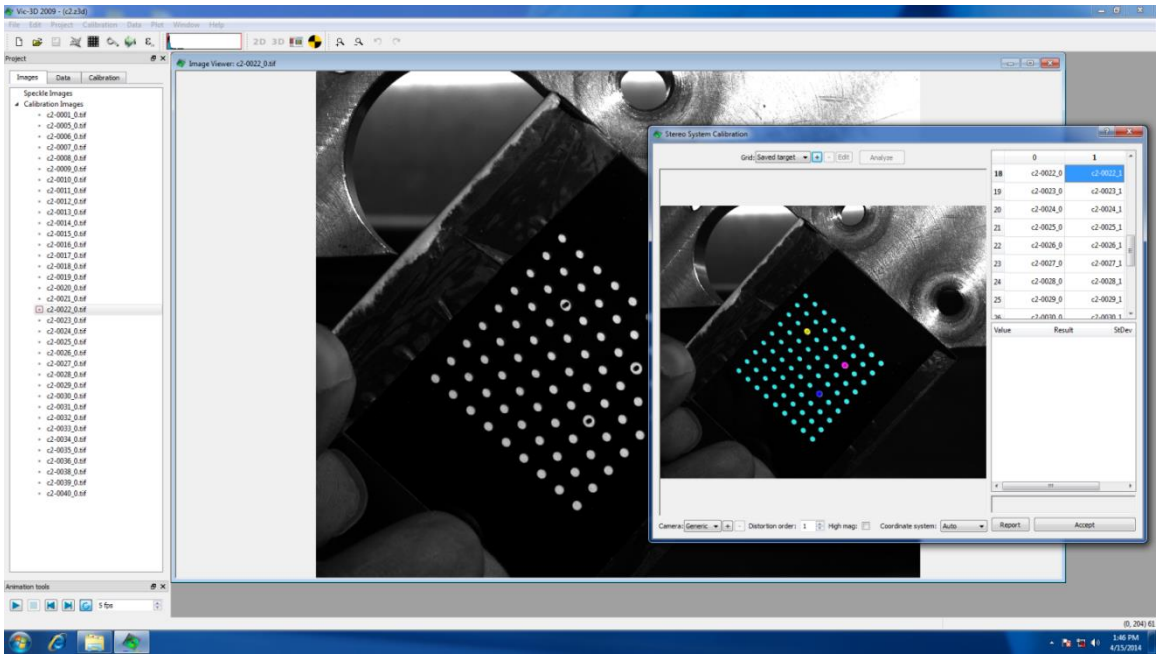

Figure 3.9: Calibration Analysis (screen shot)

Chapter 4: Finite Element Modeling of the Experiment

Finite element modeling was utilized to understand the distribution of stress within the specimen. The model was used to identify a suitable region of interest (ROI) for analysis of stress and strain by identifying regions of uniform stress. The amount of deviation caused by the use of a rectangular specimen versus a notched specimen was quantified and is discussed here in detail. The analysis helped to measure the required load to achieve target stresses in the specimen for any given orientation of loading apparatus.

MODELING OF THE TEST SETUP

The finite element software Abaqus FEA 6.13 was used for performing finite element analysis. Abaqus is commercially available and developed by Dassault Systems. In the preprocessing part, the geometry of the specimen was modeled in Abaqus/CAE. Two models were created to represent the rectangular and notched geometry of the specimens. The models are done in two dimensions. As the load is symmetric with respect to depth, a 2-D model was considered to be adequate. However, there might be some deviation along the depth of the specimen due to Poisson's effect, which was assumed to be negligible. This assumption is valid as the material was unrestrained for the deformation along the direction of depth. For this reason, no significant stress component along the specimen depth would be present on the specimen surface. The strain component along the depth measured from the actual test also supports this approximation.

In addition to the specimen, the loading apparatus was also modeled in Abaqus/CAE. To represent the Arcan apparatus, two parts of the half-circular apparatus were modeled. Then, the top and bottom part of the Arcan apparatus and the specimen in between were assembled to imitate the actual test setup. The final geometry of the setup for the notched specimens can be seen in Figures 4.1.

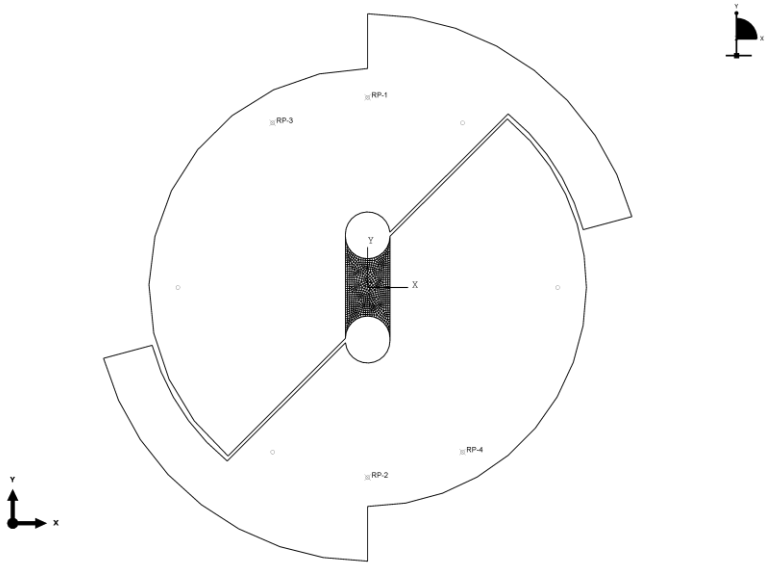

Figure 4.1: FEM model of notched specimen

For this analysis, it is assumed that the material was purely elastic without any time dependent behavior. Since the objective of this analysis was to obtain the spatial distribution of stresses across the Arcan test specimen, it was adequate to assign a unit elastic modulus as the material property. The Arcan apparatus (except the specimen) was considered as rigid. This consideration is valid since elastic modulus of aluminum (the material of the Arcan apparatus) is very high compared to that of FAM.

The applied load in FEA was kept at unity. The effect of the gravity and weight of the apparatus was also ignored for this analysis. The load was provided in 15º intervals; that is, the Arcan apparatus was rotated around the loading train so that the position of the load varied with respect to the specimen for different tests. If the load is in vertical position (at 90º with the horizontal) the result would be shear force and if the position of the load is 0º with the horizontal, then pure tension force is ensued. The loading positions in between 0º and 90º, such as, 15º, 30 º, 45º, 60 º, and 75º, result in a combination of tensile and shear load with varying proportions. With the increase of loading angle from 0º, the proportion of the shear force increases and no tensile force is present in the 90º position. However, even in absence of the external tensile force, tensile stress can be generated in the specimen due to the Poisson's effect and it can be also said for the generation of shear stress despite the absence of an external shear force.

The specimen geometry was modelled using a very fine mesh to ensure accurate spatial analysis of stress. The size of mesh was $1/20^{th}$ of the smallest sample dimension. A total of 377 elements are generated for the rectangular specimen and 301 elements are generated for the notched specimen. The element chosen for this analysis was a plane stress 4-node bilinear plane stress quadrilateral element. This is a very regular and dependable choice of element.

The bonding between the specimen and the apparatus in FEM was considered as tied which is fixed, non-slip. This consideration is also realistic as we utilized epoxy for the test which provides rigid bonding between these surfaces.

FEM VALIDATION OF STRESS UNIFORMITY

After conducting elastic analysis, the principle and shear stresses were evaluated for each of the two types of specimen. With respect to the specimen geometry, σ_{yy} represents the 'vertical' directional axial stress, σ_{xx} is axial stress in horizontal direction and σ_{xy} is shear stress in the XY plane.

For the simplicity of the representation, we only considered three locations of load: shear only (90º with vertical), 60º mixed mode of stress and 0º tensile stress condition. Results for other loading angles were what one would expect by interpolating between these three values.

In Figure 4.2, a vertical section across the middle of the specimens is taken and corresponding σ_{xx} are presented without normalization. Each specimen contributes three curves for three loading positions; 90º, 60º and 0º. It should be noted that, in Figure 4.2 (and Figures 4.3-4.7), mid-points of the two specimens (notched and rectangular) are superimposed (on X-axis representing specimen dimension); hence the curves generated from the notched specimens started after and ended before the rectangular specimen due to smaller length of the notched specimen. We can observe that at least the central 1/3 portion of the curves is reasonably flat for both curve sets indicating constant tensile stress in the XX direction. In Figure 4.3 and Figure 4.4, σ_{yy} and σ_{xy} are respectively presented for the same vertical sections for the two types of specimens. Figure 4.5, 4.6 and 4.7 show the σ_{xx}, σ_{yy} and σ_{xy} stress states in a central horizontal cross section, respectively. We can observe that stress is higher near the edges but quickly reduces and flattens.

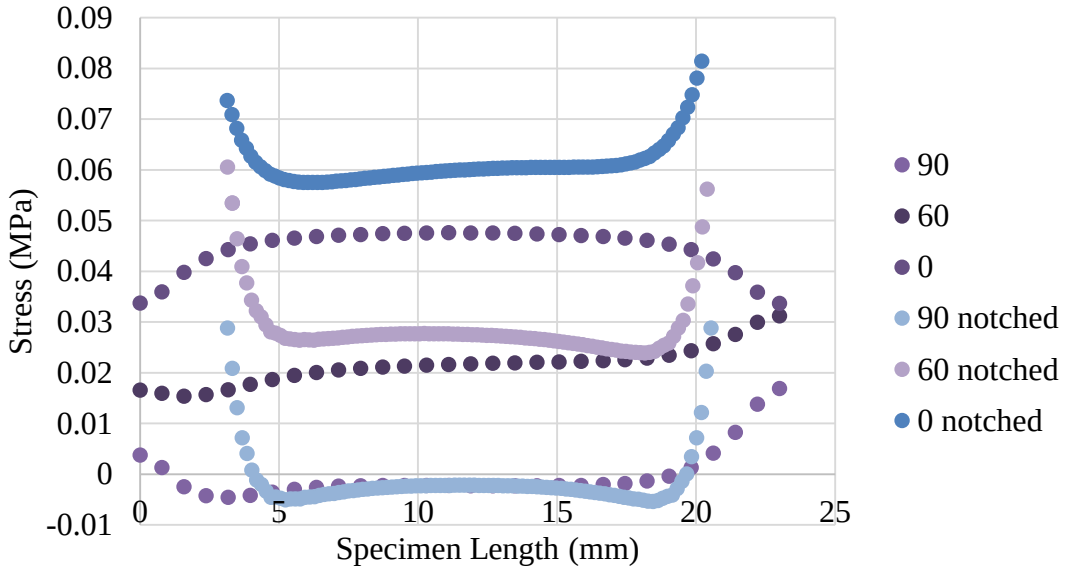

Figure 4.2: σ_{xx} in vertical cut of notched and rectangular specimen

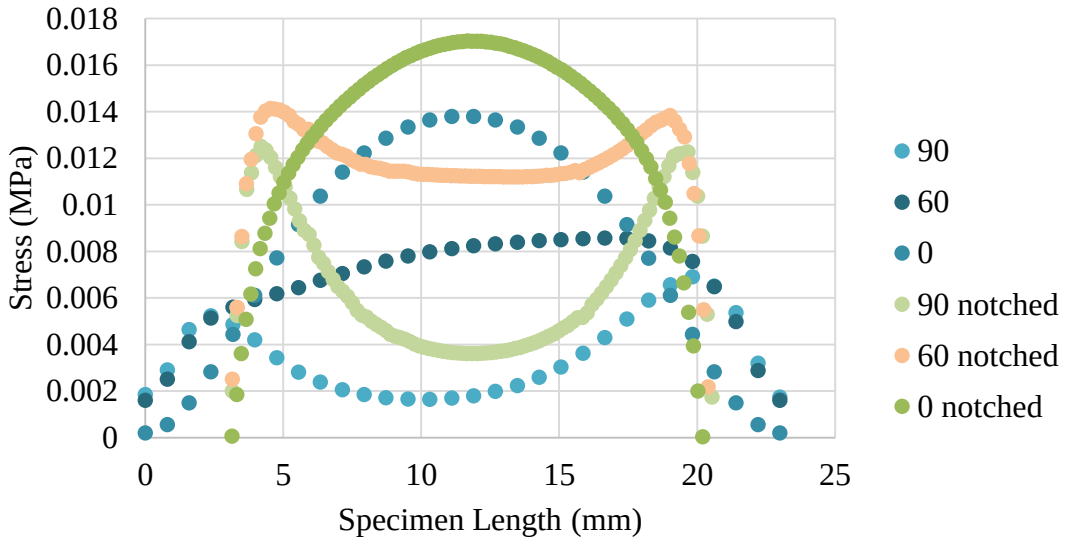

Figure 4.3: σ_{yy} in vertical cut of notched and rectangular specimen

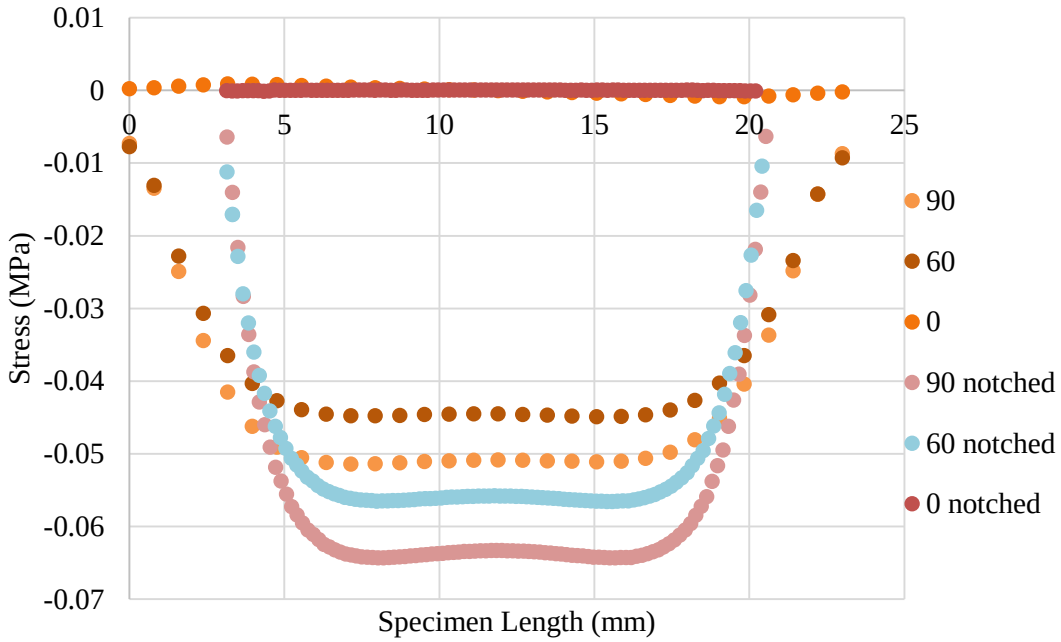

Figure 4.4: σ_{xy} in vertical cut of notched and rectangular specimen

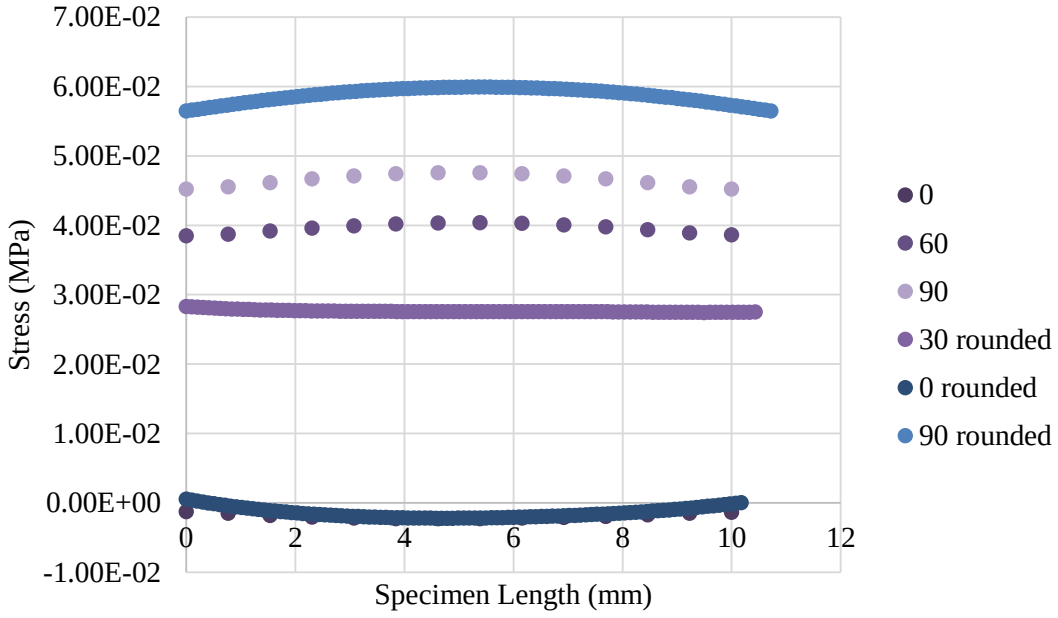

Figure 4.5: σ_{xx} in horizontal cut of notched and rectangular specimen

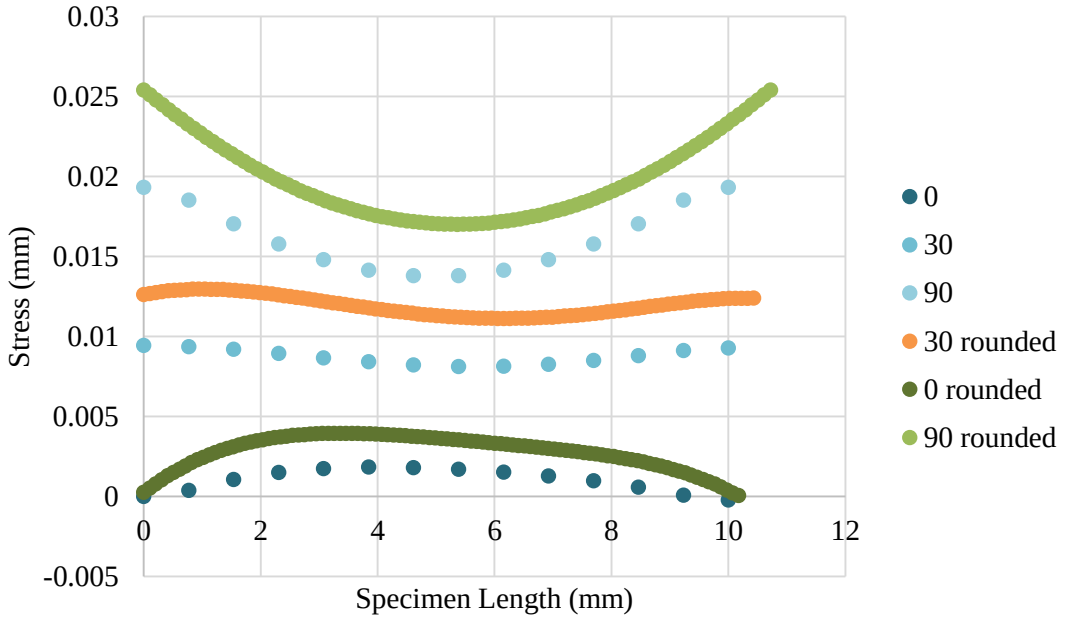

Figure 4.6: σ_{yy} in horizontal cut of notched and rectangular specimen

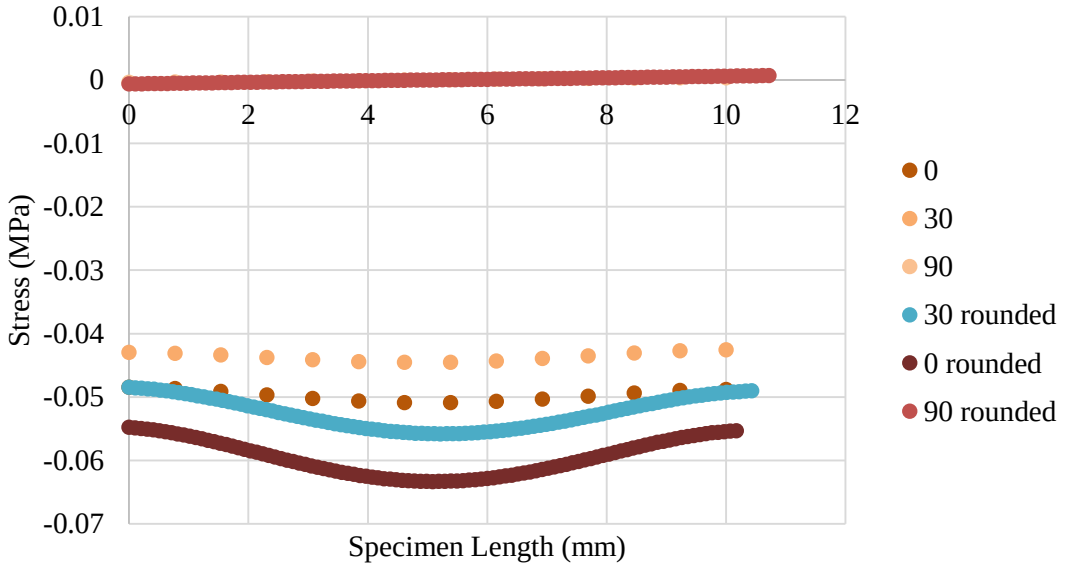

Figure 4.7: σ_{xy} in horizontal cut of notched and rectangular specimen

It can be conclude that stresses are reasonably uniform in the central 1/3 portion of the specimen when σ_{xx} and σ_{xy} are considered (Figure 4.2, 4.4, 4.5 and 4.7). On the other hand, there is significant curvature for σ_{yy} in both vertical and horizontal section (Figure 4.3 and 4.6) for both type of specimens (notched and rectangular). However, closer inspection reveals that the magnitude of such curvature is low in rectangular specimen having lower stress than the notched specimen. In addition, measurement of strain in the middle portion of the specimen would fall within the plateau of the curve, where there is less curvature. Additionally, inspection of strain in DIC is kept limited within a small central square portion (ROI) of 2 mm x 2 mm. Due to these reasons, curvature in the stress profile of σ_{yy} would not cause significant deviation from the assumption of stress uniformity in the central portion of the specimen. Hence, strain measurements near the middle of specimen should be consistent. As a result, measurement for numerous points can be taken at this region without considering the variation of strain or stress within the gage zone.

As mentioned before, we can observe better uniformity and higher stress in the notched specimen. Understandably, higher stress is due to the reduced specimen size of the notched specimen. Though better stress uniformity can be obtained in a notched specimen within a smaller length, uniform strain area is not necessary near the ends, but in the middle which was also the ROI for the analysis. We can see that both specimens provide this advantage. Hence, for the simplicity of specimen preparation and causing minimal damage during the specimen fabrication, we opted for rectangular specimen.

MEASUREMENT OF TEST PARAMETERS FROM FEM

As a unit load is applied in the FEM model along each loading direction (0º, 15º, 30º, 45º, 60º, 75º, and 90º). The spatial distribution of stresses so obtained from the analysis for any given loading direction could then be scaled with the actual load applied during the experiment to obtain actual stress distribution in the ROI of the test specimen. That is, for a given test load, we can measure the actual stress by multiplying the magnitude of the applied load with the stress obtained from FEA for the unit load. On the other hand, if it is required to develop a certain axial or shear stress in a specific orientation of load, the required test load can be obtained by dividing target stress by the stress from FEA for that same loading orientation.

It was noted at Chapter 3 that adhesion of FAM with epoxy posed a problem of stripping. For this reason, numerous specimens were tested to evaluate the load capacity of the epoxy bond of FAM with the aluminum Arcan setup. As the test primarily focuses on the effect of axial stresses on shear stress, a 45º load orientation is critical. This is because the applied loading contributes more to axial deformation than to shear below this angle (90º for full shearing load and 0º for full normal load). Hence, testing for load angles of below 45º (30º, 15º and 0º) would require a higher load for maintaining the same shear stress. For this reason, load capacity of the bond was evaluated for the 45º load orientation and shear stress was calculated for that load. The designated shear stress is 0.446 MPa and the corresponding load is 70 N. Table 4.1 summarizes the stresses for different loading orientations with constant $\sigma_{xy.}$ Required loads to maintain the given stresses are also included in the table.

An interesting observation is that the amount and proportion of change in σ_{yy} is considerably smaller than the changes in σ_{xx}. When the load acts in the YY direction (90º), it mainly produces shear stress due to the arrangement of the Arcan setup. While the load is in the XX direction (0º), it contributes to σ_{xx}. The orientations of loading in between 90º and 0º produce different combinations of shear and $\sigma_{xx,}$ with no direct load component contributing to σ_{yy}. Generation of σ_{yy} can be primarily attributed to Poisson's effect. Figure 4.8 shows the variation of σ_{xx} and σ_{yy} for a unit loading for all loading orientations. Figure 4.9 shows the variation of σ_{xx} and σ_{yy} for the adjusted loading to maintain a 0.446 MPa shear stress.

Angle	σ_{xx} (MPa)	σ_{yy} (MPa)	σxy (MPa)	Required Load (N)
Shear (90º)	-0.025	0.042	0.446	51.1
75º	0.080	0.066	0.446	52.7
60º	0.197	0.096	0.446	57.8
45º	0.364	0.115	0.446	70.0
30º	0.654	0.179	0.446	98.7
15º	1.421	0.348	0.446	190.0
Tension (0º)	-256.787	-60.764	0.446	-32769.0

Table 4.1: Stresses at the ROI of specimen at different orientations for corresponding loads

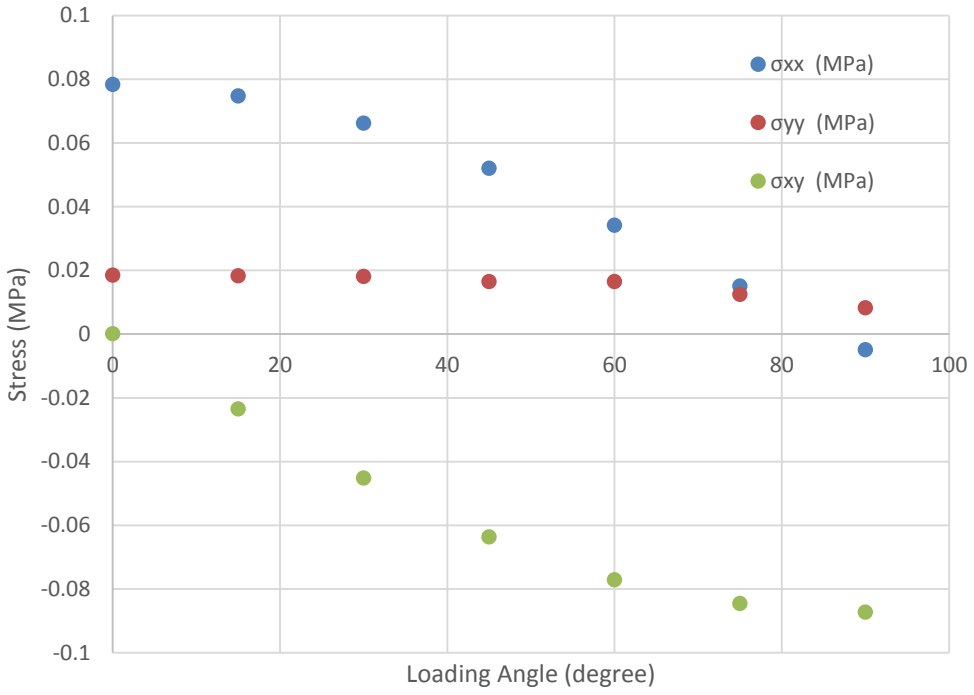

Figure 4.8: Stress vs. loading orientation (for unit loading)

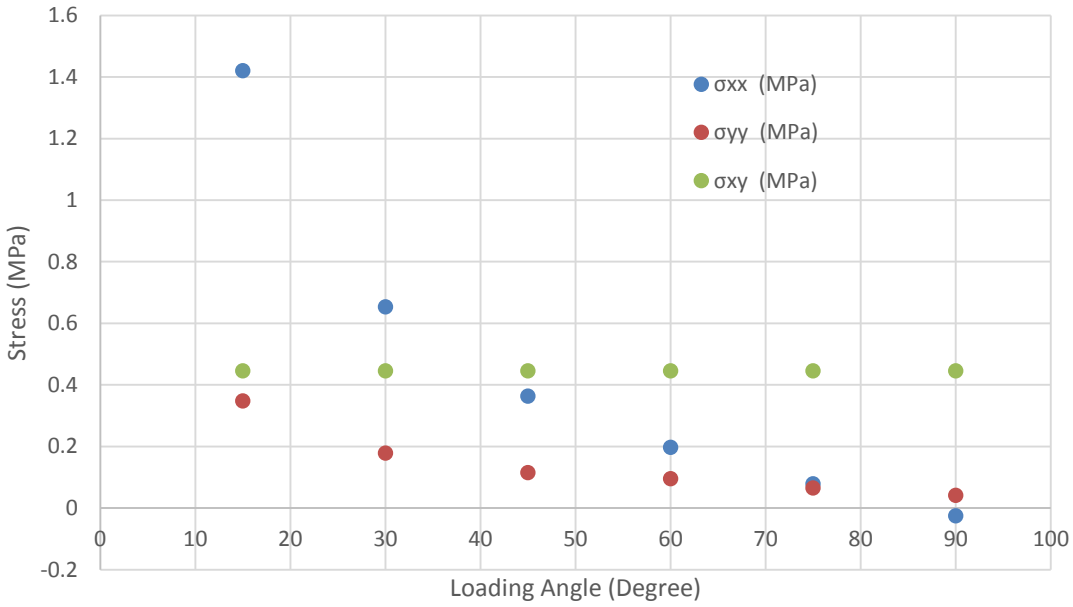

Figure 4.9 Stress vs. loading angle of Arcan Apparatus (for respective test loading)

Chapter 5: Testing and Results

The following discussion includes a comparative study of the shear strain for same shear stress but for different axial stresses for and a 45 second loading period followed by a 45 second unloading period.

As discussed in the previous chapter, results from the FEA were used to determine the applied load such that the resulting shear stress in the ROI was always the same, irrespective of the direction of loading. This was done to ensure that any observed nonlinearity could only be attributed to interaction and not inherent nonlinearity. Load orientation was changed by rotating the Arcan setup to different angles. In addition, the load magnitude for each setup orientation was altered to produce the same shear stress at the central portion of the specimen. The shear stress was of the magnitude 0.446 MPa while the magnitude of the axial stresses (σ_{xx} and σ_{yy}) varied as provided in Table 4.1 of the previous chapter. Table 4.1 also contains the required load that is to be provided by the UTM for different loading orientations to maintain the given stress levels.

Among the available loading orientations, 90º, 60º, and 45º were tested. Other loading orientations were not considered, as they would provide smaller ratios of shear stress compared to axial stresses as seen in Table 4.1. This would necessitate higher load and might cause damage to the epoxy bond between specimen and the aluminum Arcan frame as discussed in Chapter 3. In fact, we observed several bond failures at a load of 0.15-0.2 kN. Hence, we tried to ensure that the required load was kept below that level.

At the same time, we had to ensure that the amount of strain was high enough to overcome the machine noise. During trial runs, several specimens were tested at lower load magnitude compared to the test load. While the DIC system is capable of measuring smaller strains accurately, the UTM and the bolted parts of the Arcan apparatus may cause some very low amplitude vibrations. Such vibrations along with other mechanical and electrical noise can mask the actual strain at lower load magnitudes in the range of 0.005-0.02 kN. Hence, the Required Load column of Table 4.1 represents a 'checks and balances' action between the choices of the bond capacity and generation of a significant magnitude of strain. This was the rationale for selecting the loads presented in Table 4.1.

After the painted specimen was glued on the Arcan setup, the whole system was mounted on the Universal Testing Machine (UTM). An Instron UTM with a capacity of 25 kN was used. After that, we set the loading regimes as per Table 4.1 and conducted the test. The test was conducted at room temperature, which is kept at 26º±1ºC.

The testing was done for a single cycle of two steps: loading and unloading. After 2 seconds of zero loading, the load was raised to the specified level (as per Table 4.1) very quickly with rise time of 0.1 seconds. Then, the loading was sustained for 45 seconds. The load was again brought back to zero in 0.2 seconds. The recovery was monitored for another 45 seconds. After that, the test was brought to an end and the specimen was removed from the Arcan apparatus. The load vs. time relation is presented in Figure 5.1.

Only one test was conducted on each specimen. Thus, the damage incurred during the test did not propagated into future tests. However, the use of fresh specimens for each test required very accurate specimen preparation to ensure repeatability.

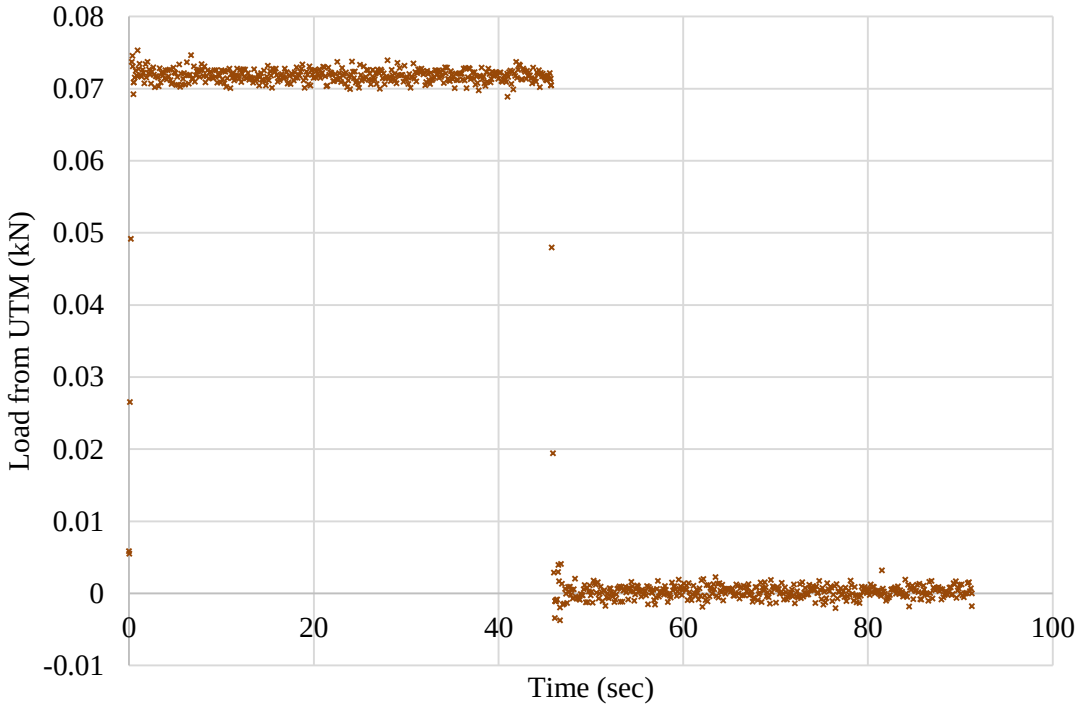

Figure 5.1: Load applied on Arcan setup from UTM for a 45º loading orientation

The DIC system captured images at a frame rate of five frames/sec. Hence, about 452 frames or data points (=90.4 s X 5 fps) are gathered from each test. These data are then analyzed using VIC-3D™ and strains were calculated for each loading case (90º, 60º, and 45º).

RESULTS OF THE ANALYSIS

Figure 5.2 demonstrates the strain profile for shear loading (90º loading orientation); that is, no axial load was provided. Test data from four specimens are presented. The strain profiles shown are for 0.446 MPa shear stress applied for 45 seconds caused by 51.1 N loading from UTM. Corresponding axial stresses are -0.025 MPa and 0.042 MPa for σ_{xx}

and σ_{yy}, respectively. Each set of four specimens underwent the same orientation in the Arcan setup and the same magnitude of loading. As we can see, they are reasonably similar to each other indicating the accuracy and repeatability of these tests.

Figure 5.3 and Figure 5.4 shows the strain profiles for 60º and 45º load orientation, respectively. For both cases, four specimens were tested and shear stress was kept constant at 0.446 MPa. However, the loads were gradually higher for 60º and 45º, 57.82 N and 70 N respectively. Respective axial stresses were also increased. σ_{xx} increased from 0.20 to 0.36 MPa when the loading angle changed from 60 to 45 degrees. σ_{yy} was also increased from 0.09 to 0.11 MPa for the same change in loading orientation.

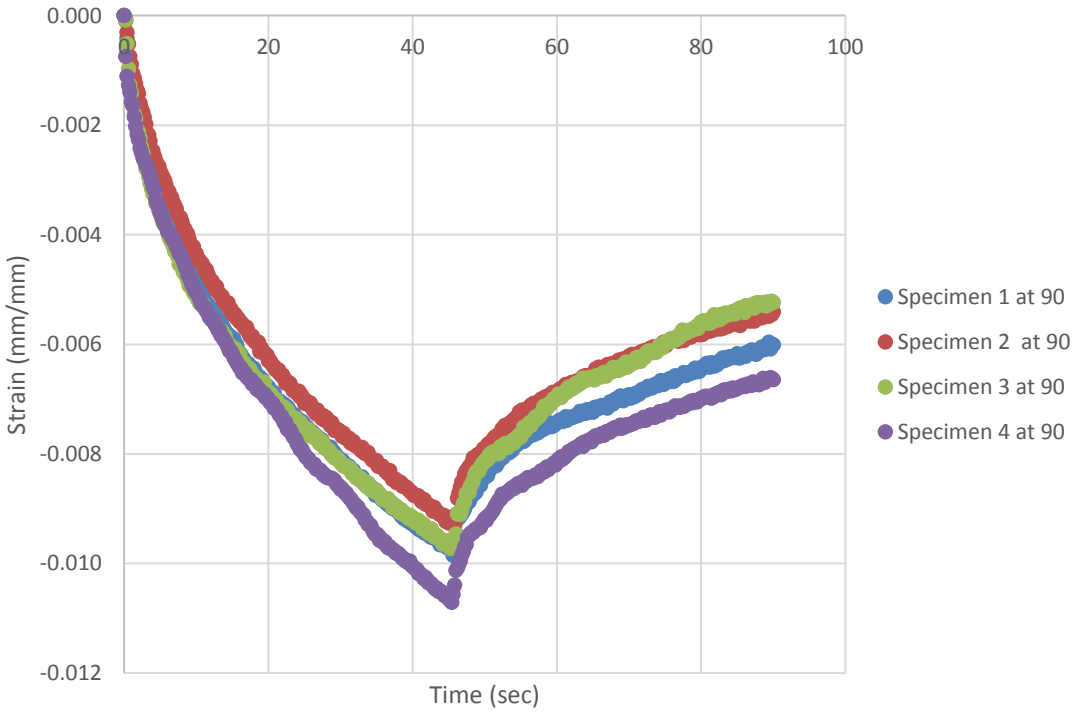

Figure 5.2: Shear strain at 90º loading orientation

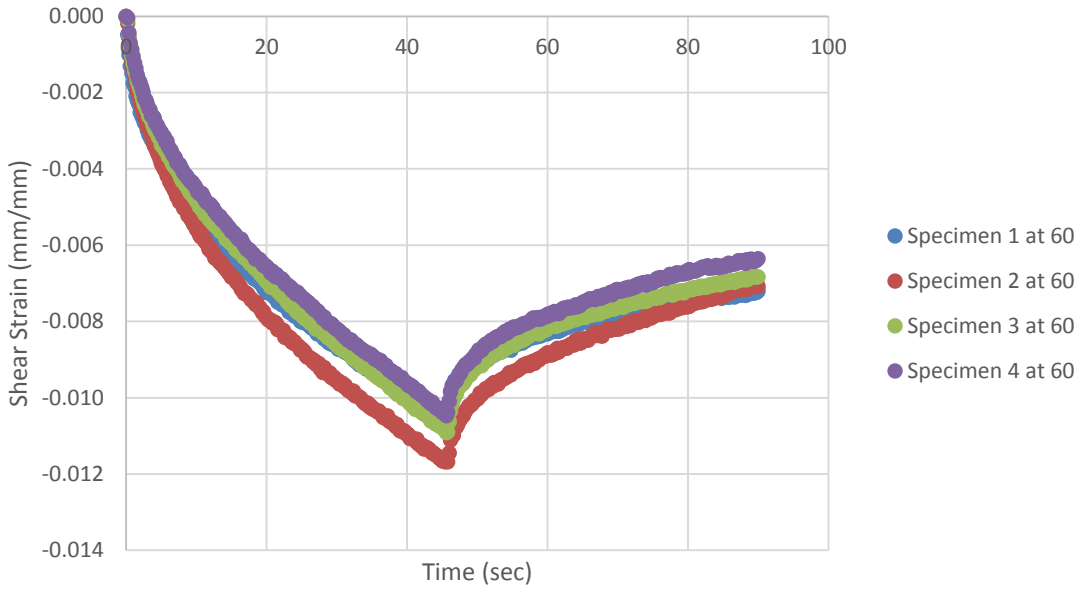

Figure 5.3: Shear Strain at 60º orientation

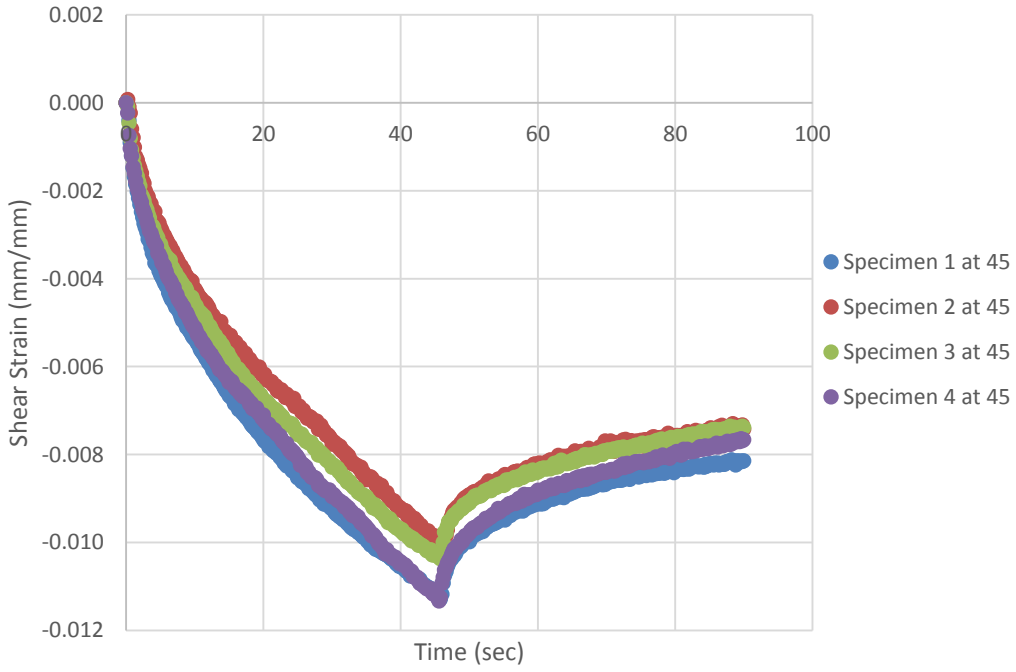

Figure 5.4: Shear strain at 45º loading orientation

Each of the shear strain values are then divided by the shear stress (0.446 MPa) to acquire shear compliance, represented by J(t). The average value of shear (creep) compliance is also measured for each loading orientation. Figure 5.5, 5.6 and 5.7 shows the shear compliances for the 90º, 60º, and 45º loading cases, respectively, along with corresponding averages. The average shear compliances are combined in Figure 5.8 which provides a fair picture about the differences between the three loading orientations. The average values of shear compliance are then fitted to two types of commonly used formulations. One is the power-law model and another is a three term Prony (Direchlet) series. The equations are presented below:

Power Law model: $J(t) = J_0 t^m$ [1]

Prony (Direchlet) Series: $J(t) = J_0 + J_1(1 - e^{-t/m_1}) + J_2(1 - e^{-t/m_2}) + J_3(1 - e^{-t/m_3})$ [2]

Here,

J_0= Glassy Compliance

J_i= Compliance for Springi

m_i = retardation times

t = loading time

i = 1, 2, 3

Microsoft® excel Solver is used for curve fitting. For equation 1, two parameters were estimated for each of the three average shear compliance curves. For equation 2, glassy

modulus was discounted and six parameters were estimated. The resultant fitted curves along with the average curves are plotted in Figure 5.9, 5.10 and 5.11 for 90º, 60º, and 45º loading cases, respectively. The estimated parameters are provided in Table 5.1.

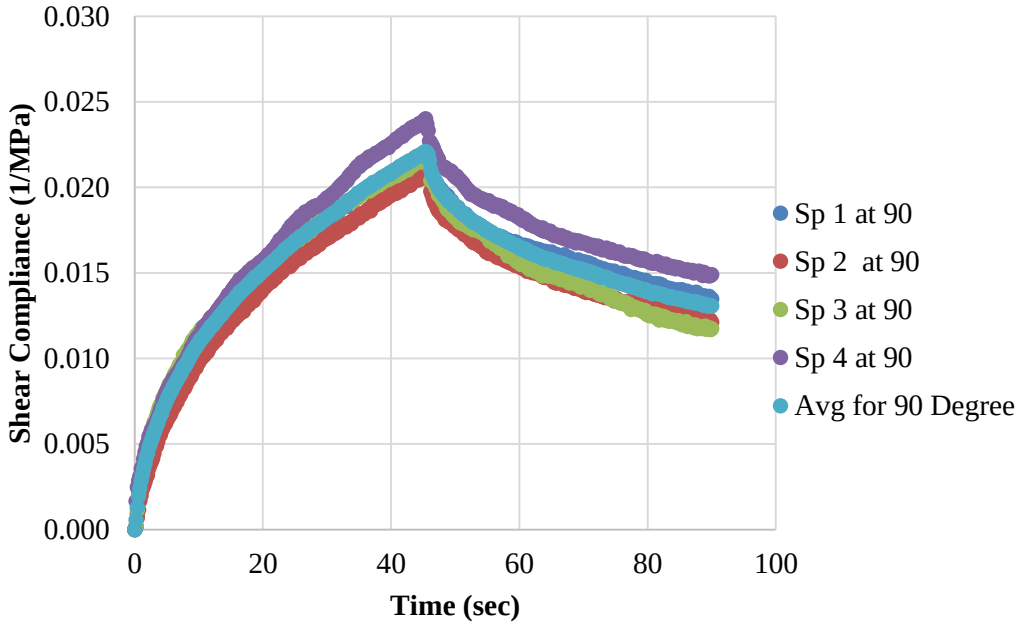

Figure 5.5: Shear Compliance for 90º

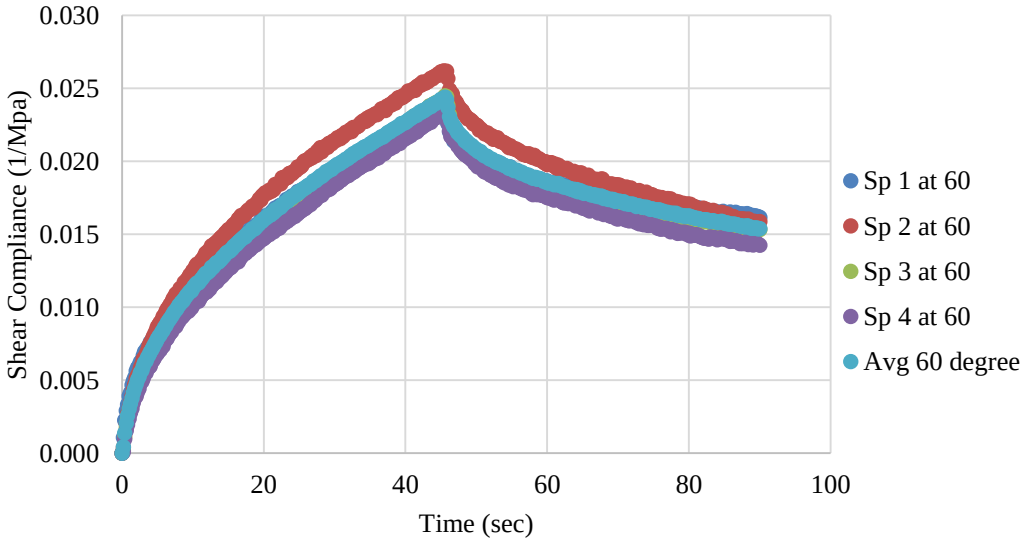

Figure 5.6: Shear compliance at 60º

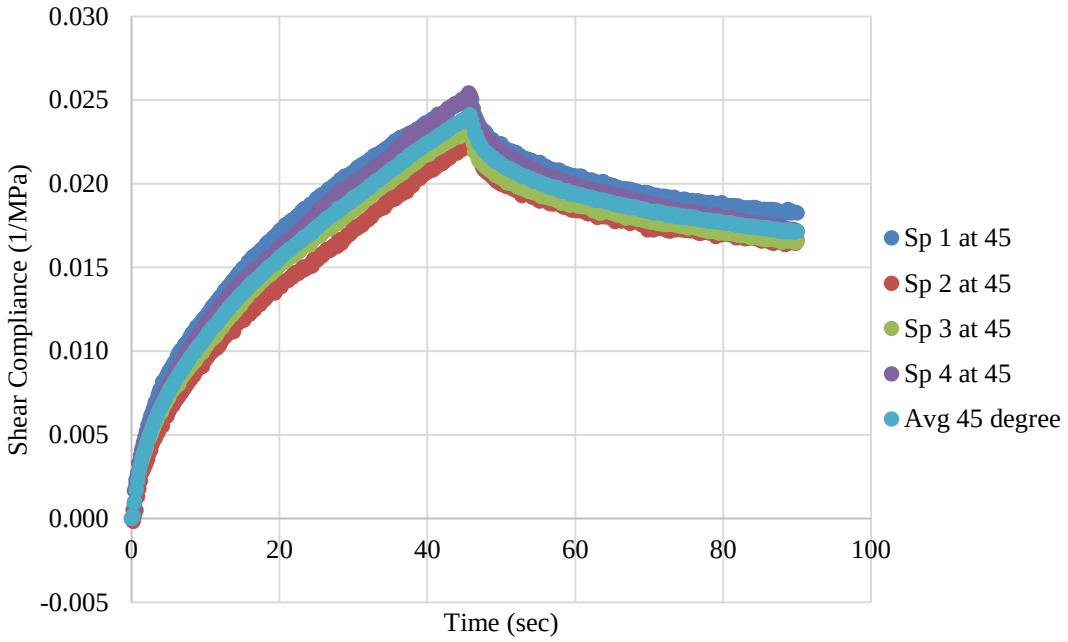

Figure 5.7: Shear Compliance at 45º

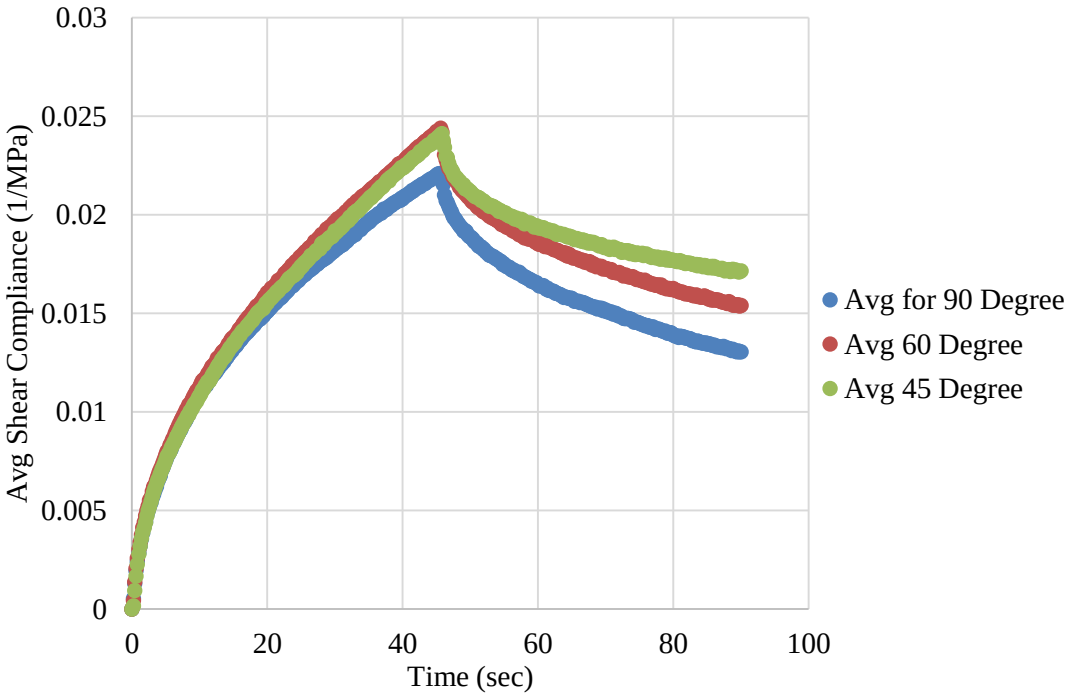

Figure 5.8: Average shear compliance for different loading orientations

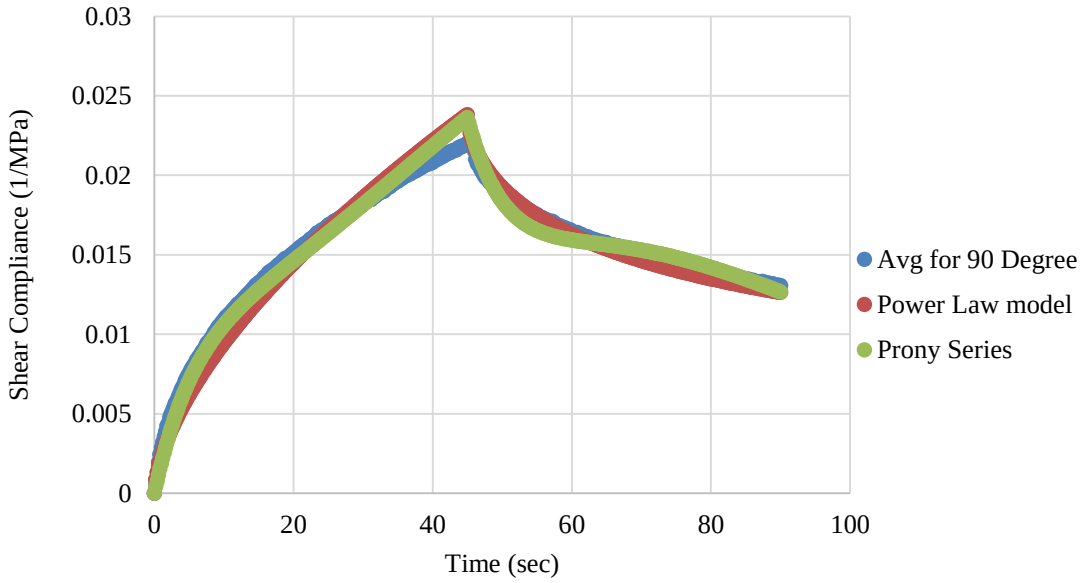

Figure 5.9: Curve fitting for average shear compliance at 90º

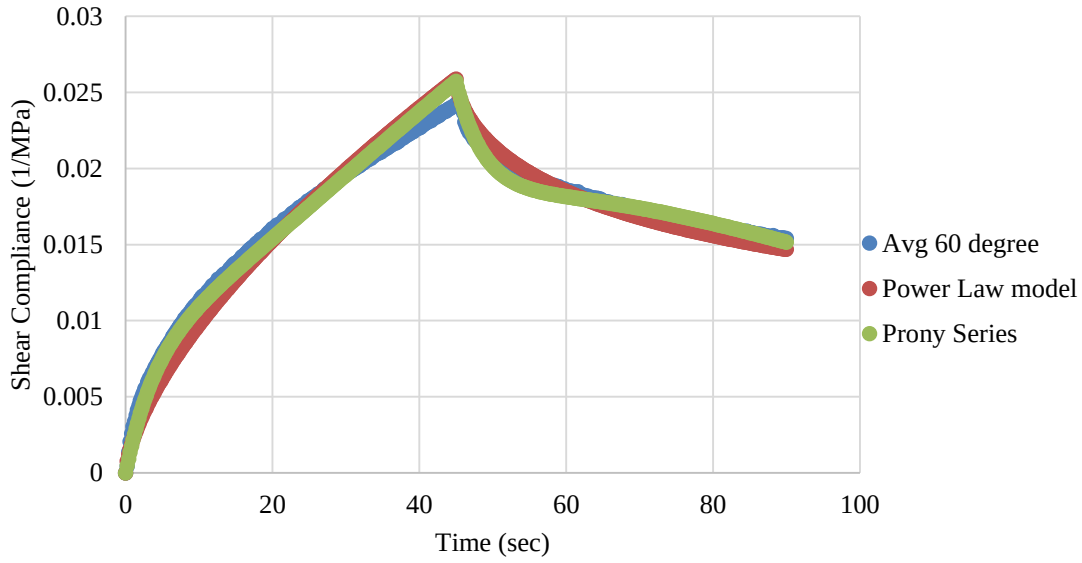

Figure 5.10: Curve fitting for average shear compliance at 60º

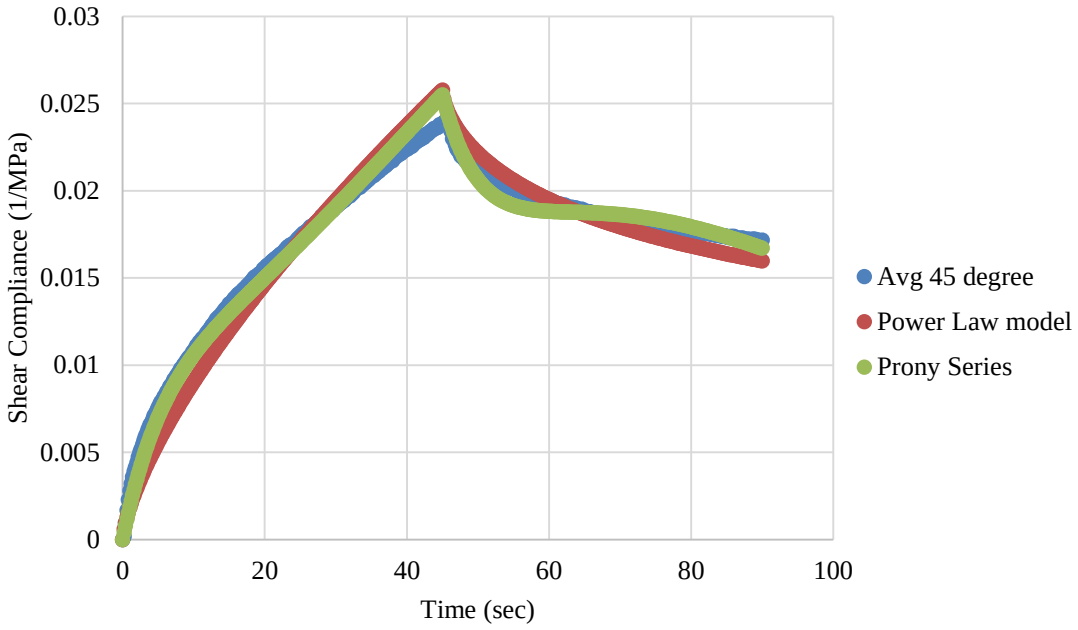

Figure 5.11: Curve fitting for average shear compliance at 45º

Load Orient.	Power Law Model		Prony Series					
	J1	m	J1	m2	J2	m2	J3	m3
90º	2.30E-03	0.613838	2.57E-01	34.74955	-0.22667	29.46122	0.014235	6.117367
60º	2.19E-03	0.648375	2.68E-01	52.64856	-0.21597	45.15966	0.008084	3.816718
45º	1.82E-03	0.696063	2.92E-01	44.46075	-0.24473	36.91352	0.011798	5.65873

Table 5.1: Estimated parameters of shear compliance from curve fitting

DISCUSSION OF THE RESULTS

We can observe in Figure 5.8 that the compliances from three different axial and shear stress combinations are very similar to each other. The compliance representing loading portions are almost identical and reach same magnitude of shear strain. However, there is

some variation in the unloading portion. Among the three compliances, the 90º orientation (shear) showed maximum recovery. As we can see, the difference in shear compliance is not significant for different types of mixed mode loading. The parameters obtained from the curve fitting are close to each other and no systemic change of parameters was observed with respect to changing magnitudes of axial stresses. This suggests that interaction non-linearity is not apparent in the FAM tested.

However, the several limitations of the study have to be taken into account. Firstly, the experiment was conducted for a fixed temperature (26º±1ºC). As asphalt is temperature sensitive, tests conducted at a different temperature might exhibit a different behavior. Another important factor was that the test was done for only one shear stress magnitude (0.446 MPa). Just like the temperature effect, it also limits the applicability of this study.

It was observed during the strain analysis using digital image correlation, that higher strain provides results that are more consistent. On the other hand, a higher degree of strain requires higher stress and hence greater loading. The specimen was relatively small and the epoxy bond of aluminum with FAM was not sufficient. This factor caused bond rupture at higher load magnitudes. Similarly, application of a very low amount of load (<0.1 kN) has a higher degree of uncertainty due to the significant proportion of machine vibration at apparatus joints from the Instron UTM which has a 25 kN operation ceiling.

In addition, the variation in the distribution of fine aggregates and asphalt in FAM would be more pronounced in a small specimen. A larger specimen can accommodate higher stresses and results would be more consistent. However, this would require a scaled up reconstruction of the Arcan setup geometry.

One of the most important concerns about the Arcan setup originates from the analysis of the fitted curves. While the fitted shear compliance curves shown in Figures 5.9-5.11 are reasonably good, they are not perfect. It should be noted that the curve-fitting was done using all data points; that is, points from the loading and unloading portions of the curve. However, if the curves are fitted only using loading or the unloading portion of the compliance, they render a perfect fit for the respective portion of the curve. The average compliance curves along with the three types of fitted curves for the Power Law model (loading + unloading points, only loading points, only unloading points) for each of the three loading orientations (90º, 60º, and 45º) are shown in Figure 5.12, 5.13 and 5.14, respectively.

When all points are used, the fitted curve show a reasonable match with the average curve with some deviation, indicating that the same parameters can express the loading and unloading portion of the compliance with reasonable accuracy. Hence, the curve fitting validates the test results.

The curves fitted using only loading points show a very good match at the loading portion, but indicates better recovery than the actual test. This phenomenon indicates that either the sample was highly damaged or there might be another stress component, which was not null during the unloading period. A probable source of stress is the Arcan apparatus. The Arcan setup is separated in two semi-circular aluminum-made parts, which are attached to the UTM load train by means of a pin for each part. The specimen, which attaches the two semicircles, transmits the load from the top half to the bottom half and support. During the unloading, the actuator of UTM does not provide any load and

hence the top half of the Arcan disk puts its weight through the specimen. This weight is a constant but it is difficult to eliminate or compensate for it. Hence, the specimen would not be in zero load during unloading and as seen in the test results, creep effects would be more pronounced for this reason (Arzoumanidis & Liechti, 2003).

The presence of interaction non-linearity was not detected for this experiment as shear compliance for pure shear and mixed-mode stress are similar. However, several limitations of the test such as the single shear stress magnitude and the single temperature used may be contributing factors that need to be considered in the evaluation.

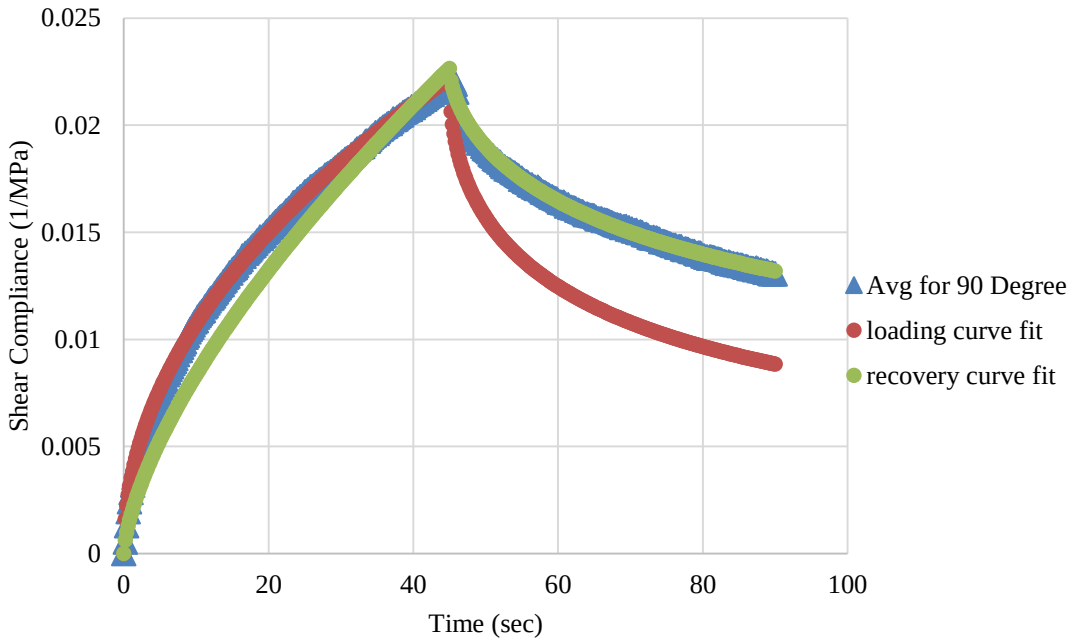

Figure 5.12: Curve fitting with loading and recovery portion at 90º

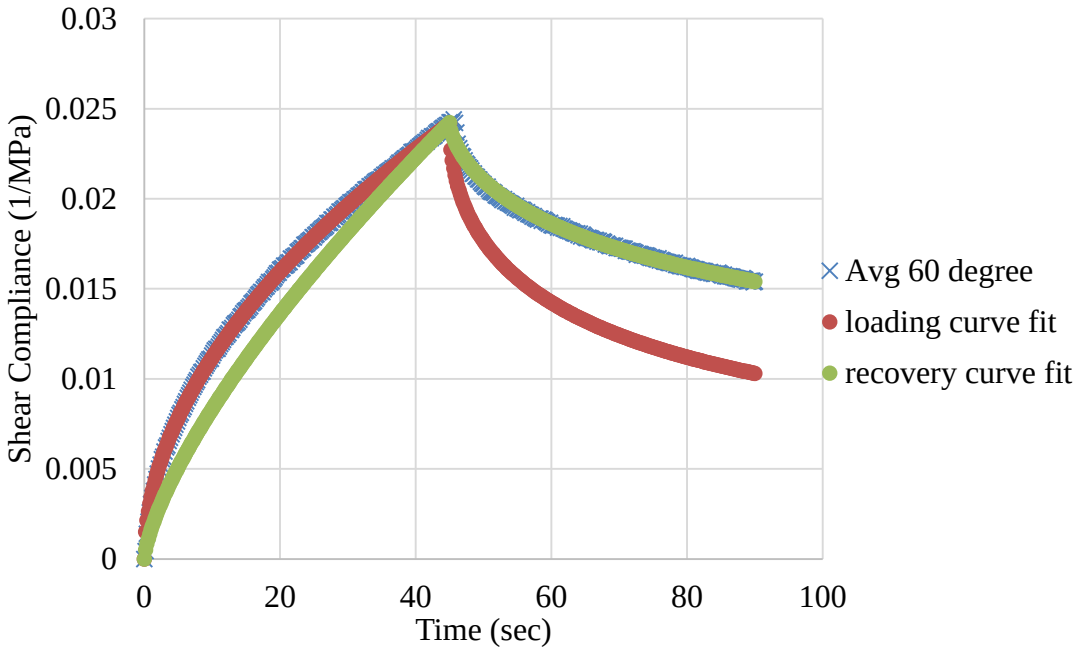

Figure 5.13: Curve fitting with loading and recovery portion at 60º

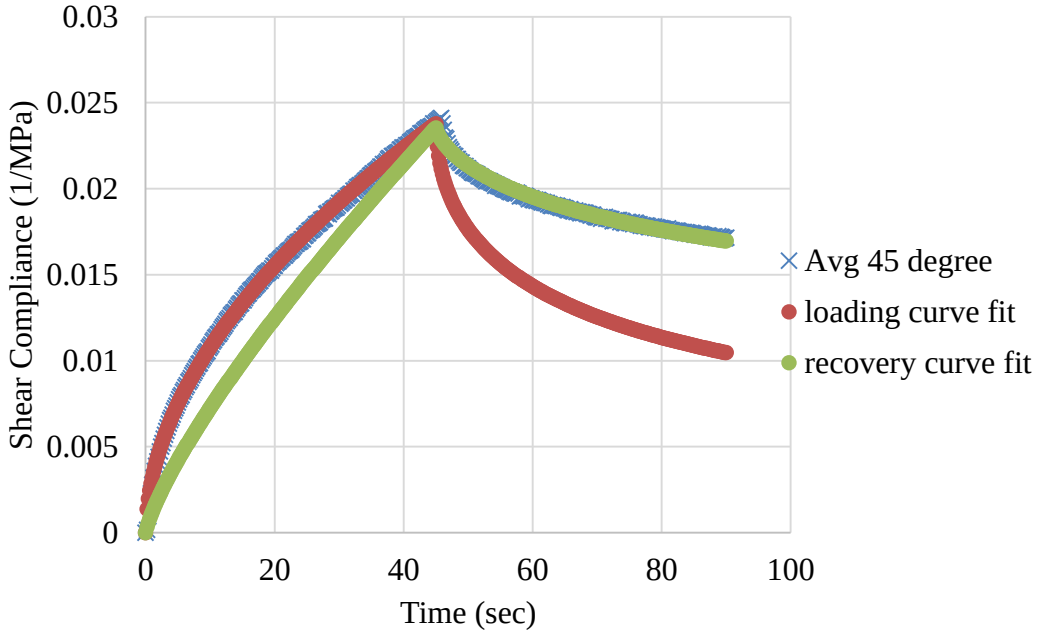

Figure 5.14: Curve fitting with loading and recovery portion at 45º

Chapter 6: Conclusions and Recommendations

This thesis addresses probable behavior alteration of fine aggregate mortar (FAM) of hot mix asphalt in shear due to the presence of axial stress. A creep-recovery test was performed on fine aggregate matrix specimens that are effectively fine aggregates and asphalt binder. The loading scenarios ensured that the specimen is subjected to different proportions of shear and axial stresses while keeping shear stress constant. Comparisons were made among shear compliance for different mixed mode conditions to identify any difference.

Mixed mode of stresses (the combination of shear and axial stress) is a significant contributor to top down cracking in pavement. Truck tires and rib effects contribute to the creation of mixed mode of stress near the surface of the pavement. Interlocked angular coarse aggregates can generate a mixed mode of stress on the FAM due to the aggregates' position (relative to FAM) and movement under wheel loads.

Researchers identified that asphalt binder can generate normal force when subjected to shear. They also found that the complex modulus of binder changed with the stress levels. However, the variation was not tested for the asphalt mortar. It created the opportunity to verify whether such variation in stress-strain relation is also present in FAM.

A special loading train, called Arcan apparatus, was used to provide the load. This apparatus, used in combination with a universal testing machine, provided the means to generate shear stress without significant bending. This system also rendered the ability to

provide axial stress along with shear. The Arcan apparatus can be rotated which provides the capability to conduct tests in different shear and axial stress combinations.

Finite element modeling was conducted to understand the magnitude of stress inside the specimen when mounted on an Arcan apparatus. The model helped to measure the shear and axial stresses; hence, required loading for each rotated loading position can be calculated while keeping the shear stress constant.

Digital image correlation, an optical measurement method, was implemented for strain measurement. This system provided the means to measure strain for the small FAM specimen without necessitating strain gages. This measurement system offers no-contact measurement with good accuracy and was thus suitable for the research objective.

The test was conducted for three loading orientations of Arcan to provide a constant 0.466 MPa shear stress combined with three different amounts of axial stresses. The tests were conducted at a temperature 26±1ºC. The measured strain profiles (with respect to time) are divided with shear stress to obtain shear compliance. Shear compliances are fitted with two types of commonly used models (power law and Prony series). After that, the shear compliances for different mixed-modes of stress are compared with each other. After evaluating the test results, we can conclude that FAM does not appear to exhibit any perceivably significant interaction non-linearity at the stress magnitude applied in this test. The variation of the shear compliance in different specimens can be attributed to the natural variability among the specimens and non-linearity present in asphalt binder. It is understood that the interaction non-linearity of the asphalt binder might not be

significant enough to alter FAM properties perceivably at the test temperature and stress levels evaluated.

In light of the presented research, a few recommendations can be made for the future research:

- The current study was done at a temperature of 26±1ºC. Since asphalt is very temperature sensitive, shear compliance for other temperatures should be evaluated.
- Tests should be done in higher and lower magnitudes of shear stress than 0.446 MPa. However, this would require a more sensitive universal testing machine and dependable epoxy to bond FAM and aluminum.
- It is necessary to work on weight reduction of the Arcan apparatus while enabling it to take larger specimens.
- The effect of shear stress variation on the tensile compliance of FAM should also be evaluated.
- Further research is required to specify the cause of variation of recovery shear compliance for different stress combinations.

References

Ann Myers, L., Roque, R., & Birgisson, B. (2001). Propagation mechanisms for surface-initiated longitudinal wheelpath cracks. *Transportation Research Record: Journal of the Transportation Research Board*, *1778*(1), 113–122.

Arcan, M., Hashin, Z., & Voloshin, A. (1978). A method to produce uniform plane-stress states with applications to fiber-reinforced materials. *Experimental Mechanics*, *18*(4), 141–146.

Arzoumanidis, G. A., & Liechti, K. M. (2003). Linear viscoelastic property measurement and its significance for some nonlinear viscoelasticity models. *Mechanics of Time-Dependent Materials*, *7*(3-4), 209–250.

Baladi, G. Y., Schorsch, M., & Svasdisant, T. (2003). *Determining the causes of top-down cracks in bituminous pavements*. Retrieved from http://trid.trb.org/view.aspx?id=875384

Canestrari, F., Ferrotti, G., Partl, M. N., & Santagata, E. (2005). Advanced testing and characterization of interlayer shear resistance. *Transportation Research Record: Journal of the Transportation Research Board*, *1929*(1), 69–78.

Correlated Solutions. (2005). VIC-3D user manual. *Columbia, SC: Correlated Solutions*.

Correlated Solutions. (2013). The VIC-3D™ Measurement System. *VIC-3D™ - Correlated Solutions*. Retrieved April 21, 2014, from http://www.correlatedsolutions.com/wp-content/uploads/2013/10/VIC-3D%20System%20Specs.pdf

Dauzats, M., & Rampal, A. (1987). Mechanism of surface cracking in wearing courses. In *INTERNATIONAL CONFERENCE ON THE STRUCTURAL DESIGN*.

Delgadillo, R. (2008). *Nonlinearity of asphalt binders and the relationship with asphalt mixture permanent deformation*. ProQuest.

Gerritsen, A., Van Gurp, C., Van der Heide, J., Molenaar, A., & Pronk, A. (1987). Prediction and Prevention of Surface Cracking in Asphaltic Pavements. In *Publication of: Michigan University, Ann Arbor* (Vol. VOLUME I, PROCEEDINGS, UNIVERSITY OF MICHIGAN,). ANN ARBOR, MICHIGAN.

Hild, F., & Roux, S. (2006). Digital image correlation: from displacement measurement to identification of elastic properties–a review. *Strain*, *42*(2), 69–80.

Huang, C.-W. (2008). *Development and numerical implementation of nonlinear viscoelastic-viscoplastic model for asphalt materials*. Texas A&M University.

Hung, S. C., & Liechti, K. M. (1997). An evaluation of the Arcan specimen for determining the shear moduli of fiber-reinforced composites. *Experimental Mechanics*, *37*(4), 460–468.

Hung, S. C., & Liechti, K. M. (1999). Finite Element Analysis of the Arcan Specimen for Fiber Reinforced Composites under Pure Shear and Biaxial Loading. *Journal of Composite Materials*, *33*(14), 1288–1317. doi:10.1177/002199839903301402

Iosipescu, N. (1967). New Accurate Procedure for Single Shear Testing of Metals. *Journal of Materials*, *2*(3), 537–566.

Izadi, A., Bhasin, A., & Motamed, A. (2011). *Designing Fine Aggregate Mixtures to Evaluate Fatigue Crack Growth in Asphalt Mixtures*. Southwest Region University Transportation Center, Center for Transportation Research, University of Texas at Austin. Retrieved from http://d2dtl5nnlpfr0r.cloudfront.net/swutc.tamu.edu/publications/technicalreports/161022-1.pdf

Lu, H., & Knauss, W. G. (1998). The role of dilatation in the nonlinearly viscoelastic behavior of PMMA under multiaxial stress states. *Mechanics of Time-Dependent Materials*, *2*(4), 307–334.

Luo, P., Chao, Y., Sutton, M., & Peters III, W. (1993). Accurate measurement of three-dimensional deformations in deformable and rigid bodies using computer vision. *Experimental Mechanics*, *33*(2), 123–132.

Matsuno, S., & Nishizawa, T. (1992). Mechanism of longitudinal surface cracking in asphalt pavement. In *International Conference on Asphalt Pavements, 7th, 1992, Nottingham, United Kingdom* (Vol. 2).

Motamed, A., Bhasin, A., & Liechti, K. M. (2011). Interaction nonlinearity in asphalt binders. *Mechanics of Time-Dependent Materials*, *16*(2), 145–167. doi:10.1007/s11043-011-9141-1

Motamed, A., Bhasin, A., & Liechti, K. M. (2012). Constitutive modeling of the nonlinearly viscoelastic response of asphalt binders; incorporating three-dimensional effects. *Mechanics of Time-Dependent Materials*, *17*(1), 83–109. doi:10.1007/s11043-012-9178-9

Myers, L. A., Roque, R., & Ruth, B. E. (1998). Mechanisms of surface-initiated longitudinal wheel path cracks in high-type bituminous pavements. *Journal of the Association of Asphalt Paving Technologists*, *67*.

Ozer, H., Al-Qadi, I. L., & Duarte, C. A. (2011a). A three-dimensional generalised finite element analysis for the near-surface cracking problem in flexible pavements. *International Journal of Pavement Engineering*, *12*(4), 407–419.

Ozer, H., Al-Qadi, I. L., & Duarte, C. A. (2011b). Effects of Nonuniform and Three-Dimensional Contact Stresses on Near-Surface Cracking. *Transportation Research Record: Journal of the Transportation Research Board*, *2210*(-1), 97–105.

Poynting, J. (1909). On pressure perpendicular to the shear planes in finite pure shears, and on the lengthening of loaded wires when twisted. *Proceedings of the Royal Society of London. Series A, Containing Papers of a Mathematical and Physical Character*, *82*(557), 546–559.

Romanoschi, S. A., & Metcalf, J. B. (2001). Characterization of asphalt concrete layer interfaces. *Transportation Research Record: Journal of the Transportation Research Board*, *1778*(1), 132–139.

Roque, R., Zou, J., Kim, Y. R., Baek, C., Thirunavukkarasu, S., Underwood, B. S., & Guddati, M. N. (2010). *Top-Down Cracking of Hot-Mix Asphalt Layers: Models for Initiation and Propagation*. National Cooperative Highway Research Program, Transportation Research Board of the National Academies. Retrieved from http://www.chinautc.com/usa/upfile/content/20101025163810812.pdf

Schreier, H., Orteu, J.-J., & Sutton, M. A. (2009). *Image correlation for shape, motion and deformation measurements: basic concepts, theory and applications*. Springer-Verlag US.

Stuart, K. D., & Mogawer, W. S. (2000, October). Modified Asphalt Binders in Mixtures - Topical Report: Permanent Deformation Using A Mixture With Diabase Aggregate. *6. Cumulative Permanent Shear Strain - Modified Asphalt Binders in Mixtures - Topical Report: Permanent Deformation Using A Mixture With Diabase Aggregate, October 2000 - FHWA-RD-02-042*. Retrieved April 20, 2014, from http://www.fhwa.dot.gov/publications/research/infrastructure/pavements/asphalt/pavepubs/02042/sect06tosect07.cfm

Sutton, M. A., McNeill, S. R., Helm, J. D., & Chao, Y. J. (2000). Advances in two-dimensional and three-dimensional computer vision. In *Photomechanics* (pp. 323–372). Springer.

Uhlmeyer, J. S., Willoughby, K., Pierce, L. M., & Mahoney, J. P. (2000). Top-down cracking in Washington State asphalt concrete wearing courses. *Transportation Research Record: Journal of the Transportation Research Board*, *1730*(-1), 110–116.

Wang, G. (2009). *Effects of truck tire type and tire-pavement interaction on top-down cracking and instability rutting*. University of Florida. Retrieved from http://etd.fcla.edu/UF/UFE0041004/wang_g.pdf

Wang, H. (2011). *Analysis of tire-pavement interaction and pavement responses using a decoupled modeling approach*. Rice University. Retrieved from https://www.ideals.illinois.edu/handle/2142/24326

Wang, H., & Al-Qadi, I. L. (2010). Near-Surface Pavement Failure Under Multiaxial Stress State in Thick Asphalt Pavement. *Transportation Research Record: Journal of the Transportation Research Board*, *2154*(-1), 91–99.

Wang, L. B., Myers, L. A., Mohammad, L. N., & Fu, Y. R. (2003). Micromechanics study on top-down cracking. *Transportation Research Record: Journal of the Transportation Research Board*, *1853*(-1), 121–133.